Jin *et al. Energy Mater.* **2025**, *5*, 500130
**DOI:** 10.20517/energymater.2025.57

**Energy Materials**

**Review**

**Open Access**

# Electrode-level strategies for high-Ni cathodes in high-energy-density batteries beyond material design

**Wooyoung Jin[#], Hyungyeon Cha[#], Sinho Choi[*], Gyujin Song[*]**

Ulsan Advanced Energy Technology R&D Center, Korea Institute of Energy Research, Ulsan 44776, Republic of Korea.
[#]Authors contributed equally.

***Correspondence to:** Dr. Gyujin Song, Ulsan Advanced Energy Technology R&D Center, Korea Institute of Energy Research, Ulsan 44776, Republic of Korea. E-mail: gyujin.song@kier.re.kr; Dr. Sinho Choi, Ulsan Advanced Energy Technology R&D Center, Korea Institute of Energy Research, Ulsan 44776, Republic of Korea. E-mail: schoi@kier.re.kr

**How to cite this article:** Jin, W.; Cha, H.; Choi, S.; Song, G. Electrode-level strategies for high-Ni cathodes in high-energy-density batteries beyond material design. *Energy Mater.* **2025**, *5*, 500130. https://dx.doi.org/10.20517/energymater.2025.57

**Received:** 12 Mar 2025 **First Decision:** 9 May 2025 **Revised:** 20 May 2025 **Accepted:** 28 May 2025 **Published:** 26 Jun 2025

**Academic Editor:** Wei Tang **Copy Editor:** Fangling Lan **Production Editor:** Fangling Lan

## Abstract

Global electrification has been realized through lithium-ion battery system by extending its application into large-scale devices and energy storage systems. Besides, economic regulations, such as those related to climate change and carbon neutralization, have accelerated the dissemination of battery chemistry for substitution of fossil fuels. As the battery application is widely expanded into large-scale system, additional requirements such as high-energy-density and long-term cycle stability have emerged, leading to the exploration of advanced battery materials and systems beyond conventional configuration. Thus, high-Ni cathode has attracted attention owing to higher specific capacity and unexpected issues arising from structural imperfection have been recently addressed through structural carving of materials. However, to deeply investigate battery systems using high-Ni cathodes, the perspective should be extended beyond the material to the electrode level. In this paper, emerging issues and systematic strategies for the advanced high-Ni cathode at the electrode level are reviewed to provide insight into compatible electrode/material design and highlight practical development toward high-energy-density batteries.

**Keywords:** High-Ni cathode, high-voltage, high-loaded electrode, high-energy-density, lithium batteries

## INTRODUCTION

Lithium-ion batteries (LIBs) have emerged as a cornerstone in modern energy storage systems (ESSs), powering everything from portable electronics to electric vehicles (EVs) and large-scale ESSs for renewable energy grids[1-3]. The energy density, safety, and lifespan of LIBs are significantly influenced by the cathode material, which serves as the primary host for lithium (Li)-ion insertion and extraction during charge and discharge cycles[4-6]. Aside from such performance indicators, cathode materials play a critical role in determining cost and supply chains because raw materials consist of host structures. The bar graph in Figure 1A illustrates the breakdown of cell costs and mass distribution, emphasizing the significance of materials in determining overall production expenses and weight[7]. The detailed distribution reveals that the cathode is the most expensive component contributing 49.5% to the material cost, while the anode, electrolyte separator, and cell housing contribute 14.3%, 4.8%, 17.5%, and 13.9%, respectively. In terms of mass, the cathode also constitutes a significant portion along with cell housing, followed by the anode, separator, and electrolyte. These results highlight the dominant role of the cathode in influencing both cost and weight, underscoring the importance of optimizing cathode material for cost-effective and lightweight battery design. Over the past several decades, a wide range of cathode materials such as layered oxides such as lithium cobalt oxide ($LiCoO_2$, LCO), lithium nickel cobalt manganese oxide [$LiNi_xCo_yMn_zO_2$ ($x + y + z = 1$), NCM], spinel oxides (lithium manganese oxide, $LiMn_2O_4$, LMO) and olivine-type polyanionic compounds (lithium iron phosphate, $LiFePO_4$, LFP) have been developed to meet the growing demands for the improved battery performance[8,9]. Meanwhile, emerging cathodes, such as $Li_{1+n}M_{1-n}O_2$ (LMR) and $LiNi_{0.5}Mn_{1.5}O_4$ (LNMO), require further advancements in material design and supporting cell components (e.g., electrolytes and separators) and are not expected to significantly influence the EV market before the late 2020s. Accordingly, significant research efforts have been made; however, challenges remain in terms of cost, resource availability, and electrochemical degradation, particularly in applications requiring high-energy-density[10].

In order to design high-energy LIBs, nickel-based (Ni-based) materials have firmly established their position because of their higher energy density and specific energy compared to other commercialized cathode materials [Figure 1B][7]. Note that the values were calculated based on their specific capacity (mAh $g^{-1}$), average discharge potential (V *vs.* $Li/Li^+$), and electrode density (g $cm^{-3}$) and NCA-80 and ultrahigh Ni indicates $Li[Ni_{0.8}Co_{0.15}Al_{0.05}]O_2$ and $Li[Ni_{1-z}M_z]O_2$, $z \leq 0.1$ (M = transition metal), respectively.

Moreover, they are regarded as promising cathode materials due to their potential for further increasing energy by simply controlling the nickel (Ni) content. In addition to intrinsic material performance, regulatory frameworks across major global markets have emerged as a key driver for the widespread adoption of high-Ni cathode materials. In Europe, $CO_2$ emission limits for passenger vehicles mandate a 55% reduction by 2030, compelling automakers to adopt long-range battery packs with high-Ni chemistry cathode materials[11]. In China, the extension of new energy vehicle (NEV) purchase-tax exemption through 2027 continues to incentivize the deployment of long-range, high-energy EVs[12]. Concurrently, updated Ministry of Industry and Information Technology (MIIT) battery standards and EV100 programs are establishing their performance benchmarks[13]. These regulations are accelerating the adoption of ternary cathode materials with specific capacity of ≥ 240 mAh $g^{-1}$ while gradually phasing out lower-energy alternatives. In the United States, the Inflation Reduction Act (IRA) provides tax credits of up to $45 per kWh for battery cells and cathode materials produced domestically[14]. These trends have catalyzed major investments in high-Ni content of 80%, and 90% supply chains and intensified research on cobalt-lean, high-Ni cathodes to lower costs[15]. Collectively, these regulatory and economic frameworks are accelerating both commercial deployment and research focus on high-Ni cathode technologies, underscoring their central role in the global transition to low-carbon energy systems.

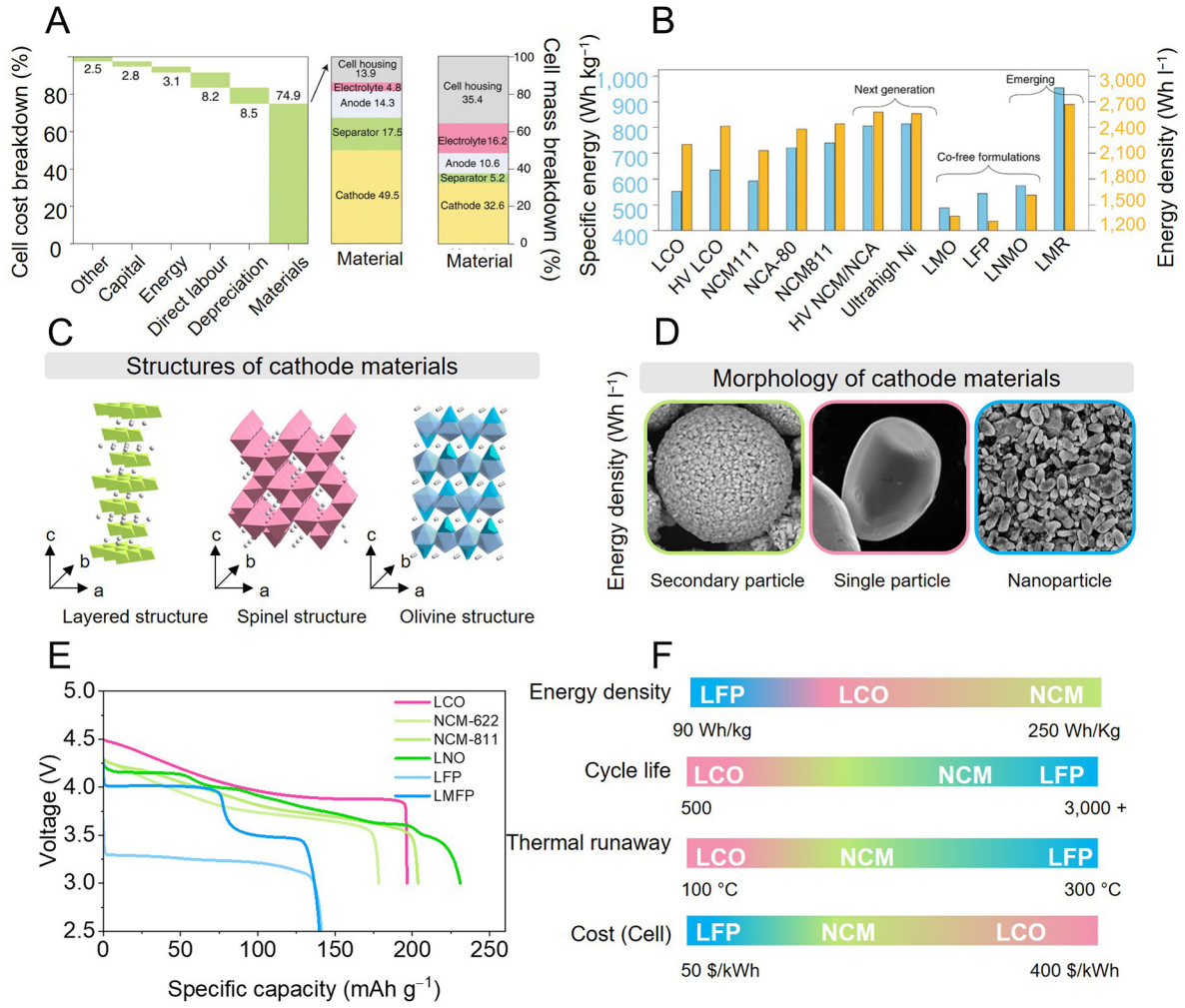


**Figure 1.** Commercialized cathode materials for LIBs. (A) Cell cost/mass breakdown of conventional LIBs cell. Current collectors are included in cell housing. Reproduced with permission[7]. Copyright 2020, Springer Nature. (B) Specific energy and energy density of various fully or partially commercialized, next-generation, and emerging cathode materials for LIBs. Reproduced with permission[7]. Copyright 2020, Springer Nature. (C) Crystal structures of intercalation cathodes for LIBs. (D) Scanning electron microscopy (SEM) images of conventional cathode particles. (E) Voltage profiles of discharging process of various cathode materials in half-cell configuration[28-32]. (F) Comparison of battery indicators of LCO, NCM, and LFP cathodes.

Aside from the material design, alternative approaches beyond Ni-based material design have also gained significant attention for increasing energy density while maximizing the use of Ni-based materials. For example, thick electrodes based on dry processing methods have emerged[16,17]. Dry processing methods, which eliminate the use of solvents in the cathode fabrication process, are considered highly promising. These methods typically use commercially available cathode material, but achieve substantially higher energy densities, which is an unattainable value with traditional wet casting process[18]. Correspondingly, several studies have proposed lowering Ni content to improve material stability while achieving high-energy-density at the electrode level. In addition to innovations in materials and electrode design, controlling the operating voltage is another strategy for enhancing energy density[19,20]. As such diverse approaches are explored, relying solely on active material-based approaches to achieve high-energy-density has reached its limitations. Furthermore, new challenges to Ni-based materials continue to be addressed, prompting further investigation from multiple perspectives[21].

Hence, this review aims to provide an in-depth perspective on the current progress and challenges of Ni-based cathodes beyond the material level and suggest key considerations for developing Ni-based cathodes with high energy. In Section "INTRODUCTION", we will cover successfully commercialized cathode material with the introduction of Ni-based material. Next, challenges and strategies for the high-energy Ni-based cathode materials will be addressed in Sections "DEVELOPMENT OF CATHODE MATERIALS" and "CHALLENGING ISSUES OF HIGH-NI CATHODES", respectively. Finally, through a comprehensive discussion, this work seeks to identify key directions for the development of next-generation cathode materials that align with sustainable and high-performance energy storage technologies.

## DEVELOPMENT OF CATHODE MATERIALS

Cathode materials are generally classified into three main crystal structures: layered, spinel, and olivine [Figure 1C][22]. LCO and NCM belong to the layered structure where the lithium (Li) and the transition metal (TM) form alternating layers, each coordinated by oxygen atoms in a tetrahedral or octahedral arrangement. Thus, two-dimensional channels within this structure enable fast Li-ion diffusion. LMO adopts a spinel structure, where $MnO_6$ octahedra share edges with $LiO_4$ tetrahedra to form a three-dimensional channel for Li-ions. Lithium manganese iron phosphate [$LiMn_xFe_yPO_4$ (x + y =1), LMFP] exhibits olivine structures, in which $MO_6$ (M = Mn or Fe) octahedra and $PO_4$ units form corner-sharing network, while $LiO_6$ octahedra share edges with $MO_6$, providing one-dimensional Li-ion diffusion channel. Considering such intrinsic properties, each material has been tailored to adopt the most favorable morphology. The morphological images in Figure 1D show representative cathode particle morphologies. LCO is typically synthesized at high temperatures (> 900 °C) using a solid-state method[23], resulting in a single-crystal morphology. In contrast, NCM is generally produced through co-precipitation methods, forming secondary particles[24]. LFP is commonly synthesized via hydrothermal methods, and due to its intrinsic low electronic conductivity issues, it is often synthesized as nanoparticles to achieve decent performance[25]. Recently, various researchers have focused on leveraging the advantages of different morphologies, such as synthesizing NCM in a single-crystal structure and developing micro-sized LFP particles to increase electrode density depending on their applications[26,27].

Successfully commercialized LCO, NCM, and LFP have been applied to various applications in our lives, and their basic electrochemical properties are shown through the voltage profiles of selected cathode materials in half-cells [Figure 1E]. The voltage profile provides critical information such as operating voltage, capacity, and phase transition behavior. These data are essential for determining energy density and gaining a deeper understanding of the electrochemical reaction mechanism of the material. As seen in voltage profiles, LCO, NCM, and LFP show quite different behaviors. LCO delivers a high discharge voltage plateau but suffers from limited cycle life due to its structural degradation during cycling. In addition, the cell price has been increasing due to the high cost of cobalt (Co), its limited availability, and the small-scale production structure. In contrast, NCM exhibits higher specific capacities which lead to higher energy density (up to 300 Wh $kg^{-1}$) with stable cycle life. LFP stands out for its remarkable safety and cycle life, enduring 3,000 cycles. Furthermore, despite its lower energy density and operating voltage, its exceptional longevity and safety make it attractive for cost-sensitive markets. Such trade-offs for each material emphasize the need for tailored cathode selection depending on the applications, and specific requirements such as safety, longevity and cost-efficiency [Figure 1F, Table 1][28-32].

One of the biggest markets for LIBs is currently EVs and the steep upward trends in global EV stock underscores the accelerating demand, driven by policy changes, consumer preferences and technological advancements [Figure 2A][7]. Correspondingly, the market share for the high Ni-based material is remarkably increasing. Figure 2B shows a gradual shift towards high Ni materials, which promise higher

**Table 1. Comparison of various battery indicators of LCO, LFP, and NCM[28-32]**

| Cathode materials | Energy density (Wh $kg^{-1}$) | Cycle performance (n) | Operating voltage (V) | Thermal stability (°C) | Cost ($/kWh) |
|---|---|---|---|---|---|
| LCO | 150-200 | 500-1,000 | 3.8 | 150 | 100-400 |
| LFP | 90-120 | 2,000-5,000 | 3.2 | 310 | 55-60 |
| NCM | 150-250 | 1,000-2,000 | 3.7 | 210 | 60-70 |

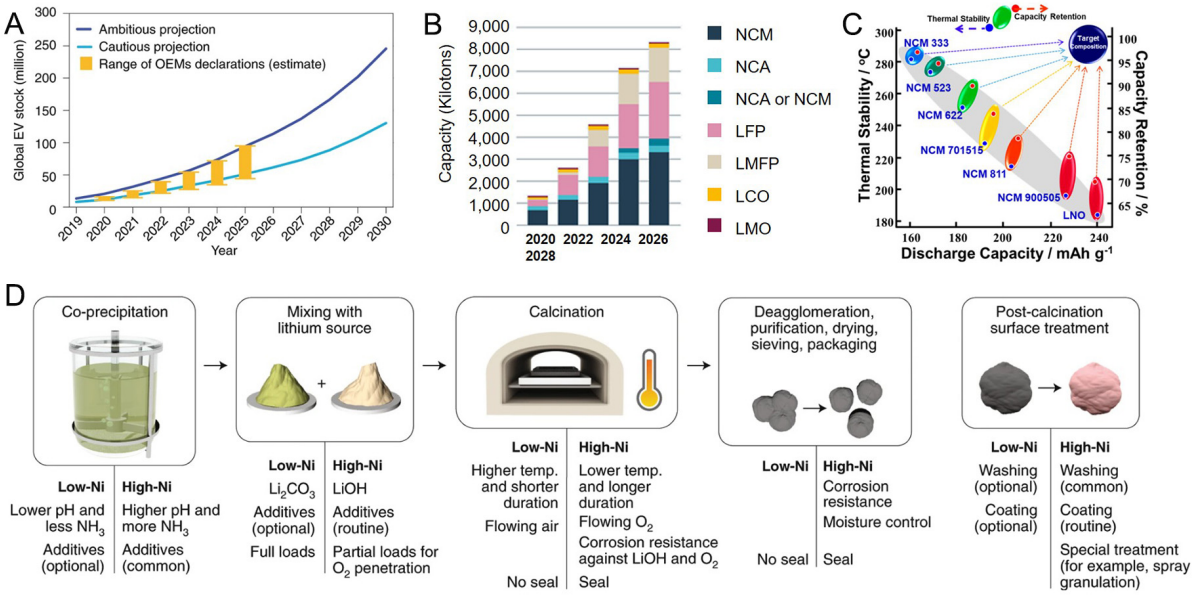


**Figure 2.** Demands and characteristics of Ni-based materials. (A) Cumulative electric vehicle deployment based on recent OEM declarations under two scenarios: cautions (new policies scenario) and ambitious (EV30@30 scenario). Reproduced with permission[7]. Copyright 2020, Springer Nature. (B) Announced cathode material production capacities by material type. Reproduced with permission[33]. Copyright 2024, Fraunhofer ISI. (C) Relationship between thermal stability, capacity retention, and discharge capacity depending on various Ni contents. Reproduced with permission[34]. Copyright 2019, American Chemical Society (D) Traditional synthesis process of Ni-based materials. Reproduced with permission[7]. Copyright 2020, Springer Nature.

energy densities[33]. Also, next-generation cathode formulations highlight efforts to enhance energy densities while reducing reliance on expensive and scarce elements such as Co. Meanwhile, other materials, such as LFP and lithium nickel manganese oxide (LNMO), maintain specific niche markets due to their cost-effectiveness and safety.

A detailed examination of various Ni-based materials shows the trade-offs also present [Figure 2C][34]. High-Ni compositions achieve discharge capacities above 200 mAh $g^{-1}$. However, these materials face critical challenges in thermal stability and cycle life, while low-Ni materials such as NCM333 exhibit excellent thermal stability and capacity retention. The production of Ni-based materials is also different from the Ni content, illustrated in Figure 2D[7]. The co-precipitation process is the conventional precursor formation method for Ni-based materials. For high-Ni systems, the process requires higher pH levels and ammonia concentrations to ensure uniform morphology and particle size. Subsequent mixing with a Li source, such as lithium carbonate ($Li_2CO_3$) and lithium hydroxide (LiOH), enables effective incorporation of Li-ions. Because of lower annealing temperature for high-Ni chemistries, LiOH with higher solubility is preferred. At the calcination step, high-Ni materials undergo lower temperatures and longer-duration heating in an oxygen-rich atmosphere. This process minimizes residual Li compounds such as LiOH and $Li_2CO_3$ and

ensures structural homogeneity. Even under well-controlled calcination conditions, the formation of residual Li in high-Ni material is unavoidable[35,36]. Therefore, thorough post-treatment is essential to prevent the exposure of moisture and corrosion. For instance, washing, coating, and special treatment have mitigated these risks by enhancing surface stability and reducing parasitic reactions until now[37,38].

## CHALLENGING ISSUES OF HIGH-NI CATHODES

### Overview of challenges in high-Ni cathodes

Since the early 2010s, increasing the Ni content has been considered the most effective strategy for improving the energy density of batteries, actively pursued by both researchers and manufacturers[39-41]. Although a higher Ni content can enhance the specific capacity, it concurrently amplifies the intrinsic structural and chemical instabilities of Ni-based materials, ultimately imposing significant limitations on battery performance[39,42-45]. Figure 3A provides a schematic representation of the critical issues associated with high-Ni materials.

Primary issue in high-Ni materials is cation mixing, which arises from the comparable ionic radii of $Ni^{2+}$ (0.69 Å) and $Li^{+}$ (0.76 Å)[46,47]. During the charging process, Li vacancies are generated, enabling the migration of $Ni^{2+}$ ions into vacant Li sites. As cycling progresses, $Ni^{2+}$ ions gradually occupy these vacancies, resulting in the transformation of the original hexagonal layered structure into a spinel-like phase and, eventually, a nickel oxide (NiO)-like phase[48]. Cation mixing is particularly evident at the particle surface region, where highly oxidized $Ni^{3+}$ and $Ni^{4+}$ ions accumulate[49]. The Li/Ni site exchange disrupts Li-ion pathways, significantly decreasing Li-ion diffusivity, resulting in capacity fading and poor electrochemical performance. With increasing Ni fraction especially above 80%, the H2-H3 phase transition occurs around 4.15 V, which is a major cause of lattice shrinkage along the c-direction[50]. Ryu *et al.* reported that reducing Ni content alleviates the phase transition, with the associated peak disappearing entirely when the fraction falls below 60%[51]. The repeated lattice expansion and contraction during cycling also affect the morphological properties called microcracks, commonly referred to as intergranular cracks. Microcrack formation causes contact loss between primary particles and blocks ion conduction pathways. Microcrack formation causes contact loss between primary particles and blocks ion conduction pathways. Residual Li compounds formed on the particle surface represent another critical issue that contributes to the long-term degradation of high-Ni materials. During synthesis, unstable lithium oxide ($Li_2O$) and the spontaneous reduction of surface $Ni^{3+}$ ions under ambient atmosphere result in the progressive formation of LiOH and $Li_2CO_3$[52]. The presence of these residual lithium compounds can trigger several detrimental effects in a battery system. For instance, $Li_2CO_3$ can react with lithium hexafluorophosphate ($LiPF_6$), generating carbon dioxide ($CO_2$) and oxygen ($O_2$) gases within the cell[35,53]. Additionally, alkaline LiOH can induce the dehydrofluorination of poly(vinylidene fluoride) (PVDF) binder, leading to slurry gelation, which significantly influences the industrial fabrication of battery electrodes[54]. For these reasons, in the industry field, quantifying residual lithium content is an essential requirement in the certificate of analysis (COA) for Ni-based materials. Furthermore, Ni-based materials, especially those with Ni content exceeding 80%, should be stored and handled in controlled-humidity environments or inert atmospheres. These issues observed in high-Ni materials are not fixed material properties but evolve dynamically during repeated cycling, particularly under elevated temperatures and aggressive charge/discharge conditions. For example, the H2-H3 phase transition at high voltages induces lattice contraction, which generates mechanical stress and promotes crack propagation. The newly exposed surface promotes electrolyte decomposition and increases the reactivity of residual lithium species, further destabilizing the cathode-electrolyte interface. The dynamic interplay of these degradation phenomena leads to cumulative damage under practical conditions, emphasizing the need for electrode designs that can withstand such complex and condition-dependent degradation behavior.

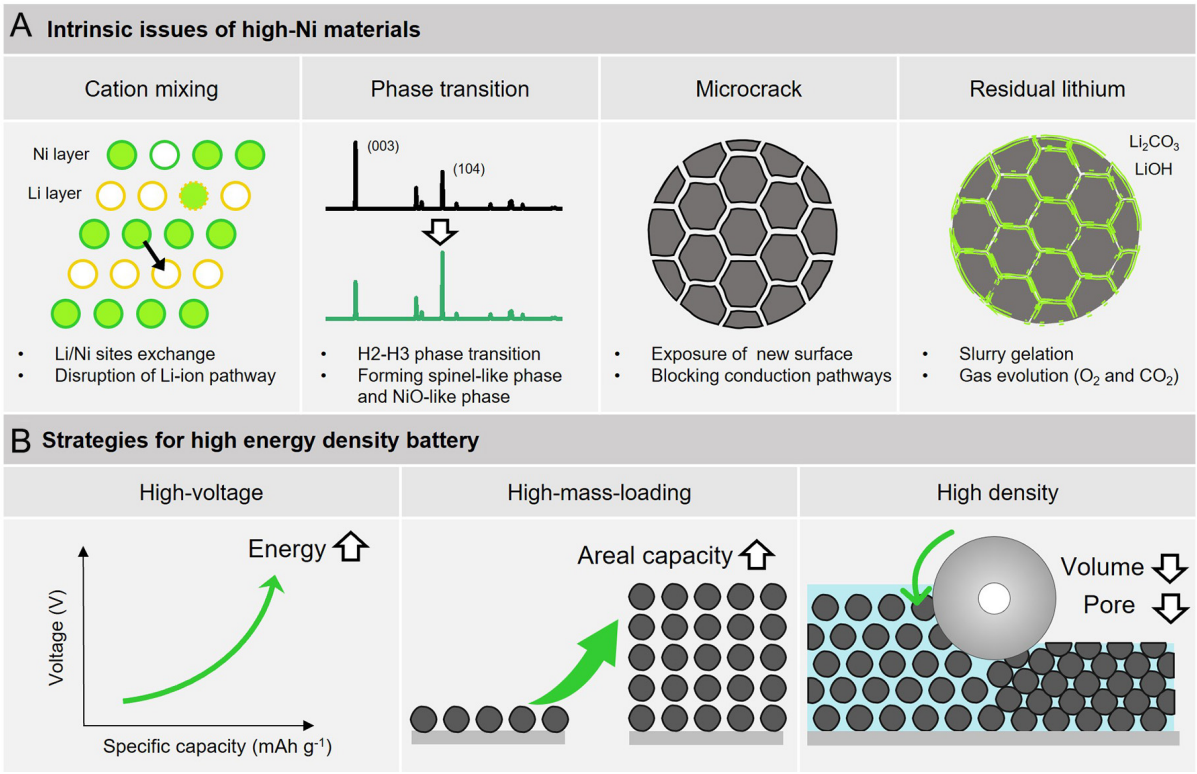


**Figure 3.** Overview of challenges and strategies for Ni-based materials toward high-energy-density batteries. (A) Addressing intrinsic issues of high-Ni materials. (B) Representative strategies for high-energy-density batteries, including high-voltage, high-mass-loading, and high electrode density.

Beyond material-level considerations, the focus shifts to strategies for enhancing energy density through electrode and cell design. To overcome the energy density limitations inherent in the chemistry of Ni-based materials, a strategic approach is required that takes into account the interplay between material chemistry and electrode design. Figure 3B illustrates various strategies for enhancing energy density using the same Ni-based materials chemistry, emphasizing the critical role of electrode and cell architecture. The equation for calculating energy density is generally defined as [Energy density (Wh $L^{-1}$ or Wh $kg^{-1}$) = Energy of cell (Wh)/Mass (kg) or Volume (L) of electrode]. Focusing on the energy term, energy density can be enhanced not only by increasing the specific capacity through a higher Ni content, but also by elevating the cut-off voltage. For example, raising the cut-off voltage from 4.3 to 4.5 V in NCM523 can simultaneously increase the operating voltage and enhance the specific capacity from 170 to 190 mAh $g^{-1}$, thereby significantly boosting overall energy density[44]. In electrode design, increasing the areal capacity is a crucial factor. Increasing the mass loading of the electrode allows for more energy storage, thereby contributing to higher energy density. Additionally, reducing the weight and volume of the electrodes is a critical factor in achieving higher energy density. Increasing electrode mass loading not only lowers the overall cell weight but also improves cost-efficiency by reducing the proportion of inactive materials, such as current collectors and separators. Furthermore, designing high-density electrodes while maintaining structural integrity is essential for enabling efficient energy storage. In the subsequent sections, we will address the emerging issues affecting overall cell performance related to design parameters of high-voltage, areal capacity, and electrode density, and discuss strategic approaches to enhance energy density.

### High-voltage operation

Ni-based materials generally operate stably at the voltage range of 3.0 to 4.3 V where the reaction potential remains within the highest occupied molecular orbital (HOMO) level of the electrolyte [Figure 4A][55]. In this range, a cathode electrolyte interphase (CEI) forms on the cathode surface, acting as a protective layer that suppresses electrolyte oxidation and enhances the electrochemical stability of the cathode materials. However, at high voltages (> 4.5 V), the oxidative stability limit of ethylene carbonate (EC)-based electrolytes is exceeded, leading to accelerated electrolyte decomposition and interfacial degradation[56-58]. During cycling, the structural degradation of Ni-based materials becomes increasingly severe, aggravating the decomposition of carbonate solvent, particularly EC, which is highly susceptible to decomposition under high potential. The oxidative decomposition of EC begins with a dehydrogenation reaction, which has a dissociation energy of -2.6 eV, making it thermodynamically favorable. The dehydrogenation of EC leads to the formation of vinylene carbonate (VC) and the accumulation of various oligomeric compounds at the interface between the cathode and electrolyte [Figure 4B][56]. These compounds, along with oxidative byproducts, can further decompose into $CO_2$ or carbon monoxide (CO) gases, worsening interfacial degradation.

Furthermore, oxidative stress at high voltages generates oxygen radicals ($O_2^{2-}$, $O_2^-$) on the cathode surface, leading to the accelerated EC decomposition, non-uniform and unstable CEI growth [Figure 4C][59]. Notably, the high oxidation states of $Ni^{4+}$ become unstable, increasing the covalency of metal-oxygen bonds and resulting in parasitic oxygen gas release. This oxygen evolution becomes particularly severe at temperatures above ~150 °C, where structural decomposition of cathode materials releases substantial amounts of oxygen[60,61]. The accumulated oxygen can react exothermically with flammable electrolyte and combustible gases, providing sufficient heat to initiate thermal runaway. Simultaneously, hydrofluoric acid (HF) molecules are usually generated through the hydrolysis of lithium hexafluorophosphate ($LiPF_6$) salt and oxidation decomposition of the electrolyte at high voltages. Dissolution of TM such as Ni, Mn, and Co is a well-known chronic problem in Ni-based materials which originates from structural degradation and HF attack[58,62]. Recent studies indicate that thermal runaway in Ni-based materials and graphite can occur even without physical failures such as separator breakdown or internal short circuits[63]. When the cell temperature surpasses approximately 115 °C due to external heating, chemical crosstalk between the cathode and anode rapidly initiates, significantly raising the internal temperature up to about 800 °C and causing battery ignition. Thus, controlling oxygen evolution and electrolyte decomposition at high voltages is critical not only for electrochemical stability but also for intrinsic safety. Given that operating Ni-based materials at high voltages is crucial for achieving high energy density, developing comprehensive strategies to simultaneously ensure cycle stability, electrochemical performance, and intrinsic safety is essential.

### High-energy-density electrode

The pursuit of high areal capacity (mAh $cm^{-2}$) has been widely recognized as a pivotal strategy to improve energy density of LIBs. Numerous studies on various cathode materials, including LFP, LCO, and NCM, have demonstrated the impact of increasing areal capacity on energy density (Wh $kg^{-1}$ and Wh $L^{-1}$) at the cell level [Figure 5A][64-66]. However, the tendency shows non-linear increase and a significant decline along with a critical threshold. This behavior can be attributed to multiple physico-chemical factors such as increase of resistance on charge pathways, ion diffusion limitations, and non-uniform electrochemical reactions within the electrode.

Typical strategies to improve areal capacity include increasing active material weight ratio and the mass loading of the electrode. Historically, research primarily focused on intrinsic properties of material chemistry and their electrochemical mechanisms, placing limited emphasis on optimizing electrode composition. Composition weight ratio of active material, conductive additive, and binder (e.g., 80:10:10 or

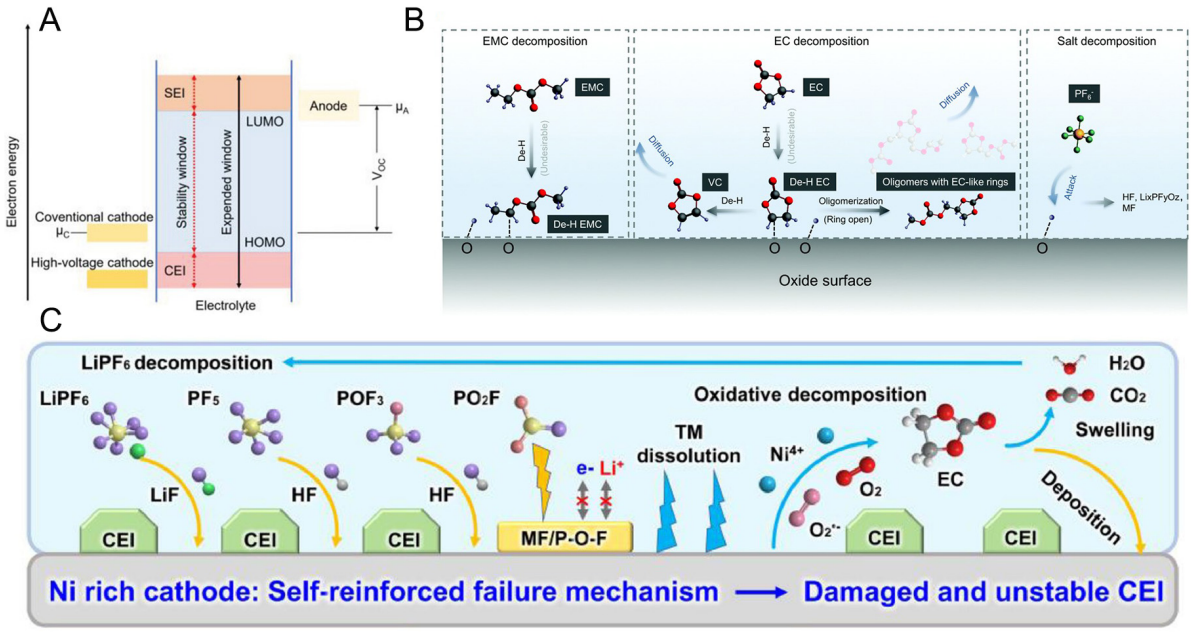


**Figure 4.** High-voltage issues for Ni-based materials. (A) Schematic diagram of electrochemical potential window of LIBs at open circuit voltage, showing stability limits of the electrolyte and electrode. Reproduced with permission[55]. Copyright 2022, Wiley-VCH. (B) Schematic illustration of the high-voltage induced oxidative decomposition mechanism of electrolyte on Ni-based materials. Reproduced with permission[56]. Copyright 2020, Royal Society of Chemistry. (C) Schematic representation of simultaneous degradation of cathode and electrolyte self-reinforced mechanism. Reproduced with permission[59]. Copyright 2021, Elsevier.

90:5:5) in conventional electrode has been recently replaced with higher active material content (> 94 wt%). This transition is particularly prominent in commercial batteries applied in EVs, significantly enhancing energy density while maintaining uniformity and stability in such compositions. Moreover, increasing mass loading also introduces significant challenges, which can reduce the relative proportion of inactive components and improve material utilization efficiency [Figure 5B][67]. However, designing thick and high-mass-loading electrode has faced limitations due to electrochemical non-uniformity and mechanical instability in electrode level [Figure 5C]. During slurry-based fabrication, solvent evaporation typically generates a density gradient and poor electrode integrity in the direction of the thickness. As a result, conductive and binder materials, featuring a solvent-favorable and low molar density, could be highly concentrated near top of electrode, while relatively heavier high-Ni active materials settle down in the bottom regions. The segregation caused by the density gradient leads to the formation of distinct carbon binder domain (CBD) migration near the surface, resulting in non-uniform ion and electron transport within the electrode[68,69].

Thick electrodes also inherently feature extended ion diffusion pathways, making ionic transport more complicated. As electrode thickness increases, electrolyte penetration becomes insufficient in the deeper regions of the electrode, leading to reaction localization near the surface. Figure 5D[70] shows the results derived from electrochemical impedance spectroscopy (EIS) measurements in symmetric cells and the transmission line model (TLM) theory for cylindrical pores, analyzing how ionic resistance ($R_{ion}$) and charge transfer resistance ($R_{ct}$) contribute differently to total internal resistance depending on electrode thickness. $R_{ion}$ shows relatively lower than $R_{ct}$ in thin electrodes, while the relative contribution of $R_{ct}$ slightly decreases as charge transfer kinetics dominate and depth-dependent delays remain minimal with increased thickness. In contrast, $R_{ion}$ becomes dominant in thicker electrodes, delaying ionic responses and reflecting its dependence on pore length. Furthermore, Park *et al.* reported that thick electrodes encountered a limitation

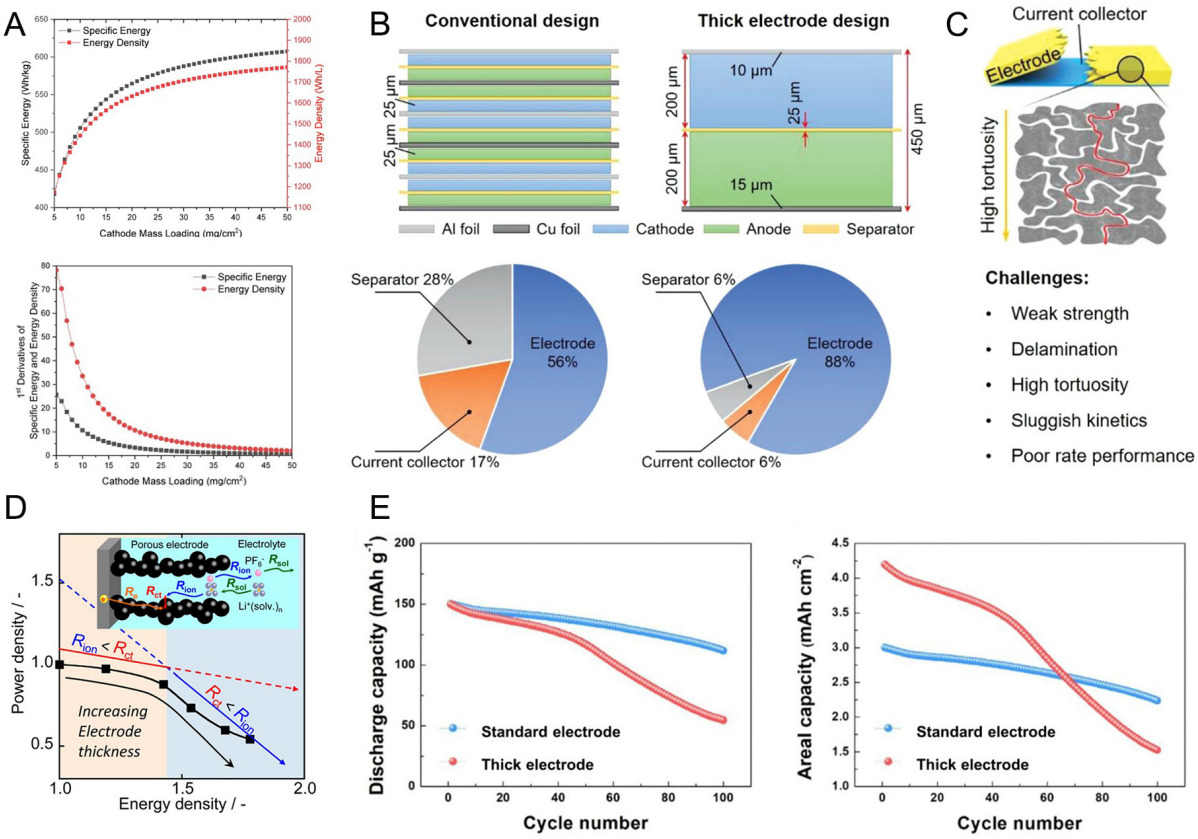


**Figure 5.** Challenges in achieving high-energy-density electrode in Ni-based materials. (A) Variation of specific energy and volumetric energy density with respect to cathode areal capacity. Reproduced with permission[66]. Copyright 2023, Elsevier. (B) Schematic illustration comparing conventional electrode design with thick electrode design. (C) Key challenges associated with thick electrode configuration. Reproduced with permission[67]. Copyright 2019, Wiley-VCH. (D) Relationship between ionic resistance ($R_{ion}$) and charge transfer resistance ($R_{ct}$) as a function of electrode thickness. Reproduced with permission[70]. Copyright 2015, American Chemical Society. (E) Comparison of cycle performance between standard and thick electrode in terms of discharge capacity and areal capacity. Reproduced with permission[71]. Copyright 2020, Elsevier.

in charge carrier mobility due to restricted Li-ion transport and electronic resistance[71]. Ion transport limitations hindered the utilization of active material near the current collector, while the top layer near the electrode/electrolyte interface remained electrochemically active at high current densities. Conversely, when electron transport was restricted, active particles near the electrode/electrolyte interface experienced higher resistance, limiting their activity, whereas the bottom layer became more active. Concurrently, the high tortuosity intensified the complexity of ion pathways, reduced the effective diffusion coefficient, and aggravated concentration of polarization[72,73]. The inhomogeneous electrochemical reactions observed in thick electrodes further complicate their performance. A notable comparison is shown in Figure 5E, where NCM622 cathodes with a standard loading of 20 mg $cm^{-2}$ and a thicker configuration of 28 mg $cm^{-2}$ (approximately 40% thicker) were compared for capacity retention. The initial areal capacity of the thicker electrode, at approximately 4.2 mAh $cm^{-2}$, significantly surpassed that of 3.0 mAh $cm^{-2}$ in the electrode with standard loading[71]. Notably, both electrodes exhibited comparable capacity retentions during the early cycles at 1C, indicating similar power densities. However, as cycling continued, the performance of the thicker electrode was remarkably degraded. After prolonged cycling, the thicker electrode retained only its initial capacity of 36%, whereas the standard electrode maintained that of 76%.

To realize high volumetric energy density (Wh $L^{-1}$), controlling the electrode volume also plays a vital role in optimizing energy storage and space utilization within the battery system. The calendering process, performed after electrode fabrication, is intended to enhance the electrical contact between particles and reduce porosity, thereby minimizing the electrode thickness and volume[74,75]. However, excessive calendering induces mechanical and structural defects in the electrode, resulting in a degradation in battery performance [Figure 6A][76]. High line pressure from cylindrical rollers generates localized stress concentrations, leading to inhomogeneous density distribution within the electrode. As a result, electrode corrugation occurs in the form of periodic waves along the calendering direction, which is further exacerbated in thick electrodes owing to its uneven compression between the coating layer and the current collector.

Figure 6B illustrates a schematic of the degradation behavior of Ni-based electrodes under high-density electrode conditions using Ni-based material[77]. According to Cha *et al.*, reaction homogeneity is maintained at a low electrode density of 3.0 g $cm^{-3}$[77]. However, at a high electrode density of 3.6 g $cm^{-3}$, polycrystalline Ni-based materials undergo non-uniform morphological evolution driven by physical and electrochemical stress, compromising cathode integrity. Scanning electron microscopy (SEM) images of Figure 6C show a magnified view of polycrystalline particles and cross-sectional electrodes near the surface layer[78]. After calendering, surface concentrated stress induces longitudinal electrode degradation. Notably, fracture of polycrystalline particles increases the specific surface area, exposing new surfaces and pores that promote side reactions and trigger additional cracking during charge-discharge cycling, significantly affecting long-term cycling performance. Moreover, the increased specific surface area enhances the hygroscopicity of the electrode, making it more susceptible to water contamination. As shown in Figure 6D, porosity and pore size within electrodes exhibit a non-linear decrease with increasing calendering intensity[79]. While macropores and mesopores diminish, the proportion of micropores (< 2 nm) increases, resulting in a high surface area and enhanced internal diffusion resistance. High calendering pressure also fractures polycrystalline structures, pushing rigid particles toward bottom side and compacting the CBD on the top layer, thereby sealing surface pores. Such damage and non-uniform pore structure not only reduce electrical conductivity but also cause imbalance in electrolyte infiltration and restrict ionic transport pathways.

Therefore, designing electrodes with higher areal capacity and density is an essential factor for developing high-energy-density batteries; however, the associated challenges such as excessive thickness and mass loading should be addressed. For Ni-based materials, it is critical to optimize electrode composition, enhance slurry processing techniques, and ensure mechanical and chemical stability. Achieving a balance between uniform electrode density and optimized material distribution is vital for unlocking the full potential of high-areal-capacity electrodes in LIBs.

### Interplay between cathode and anode (crosstalk)

The application of high-mass-loading and high-density electrodes can lead to complex chemical interactions between electrodes and electrolytes, not typically observed in coin cell configurations. A primary concern is crosstalk, where byproducts generated at one electrode migrate through the separator and trigger adverse side reactions on the opposite electrode [Figure 7A][79,80]. This phenomenon leads to non-linear cycling behavior in thick electrodes, as described in Figure 5E, showing that a sudden capacity drop occurred during the early cycle life. The issues can be categorized into TM dissolution, oxygen evolution, and electrolyte decomposition, derived from the degradation of Ni-based materials.

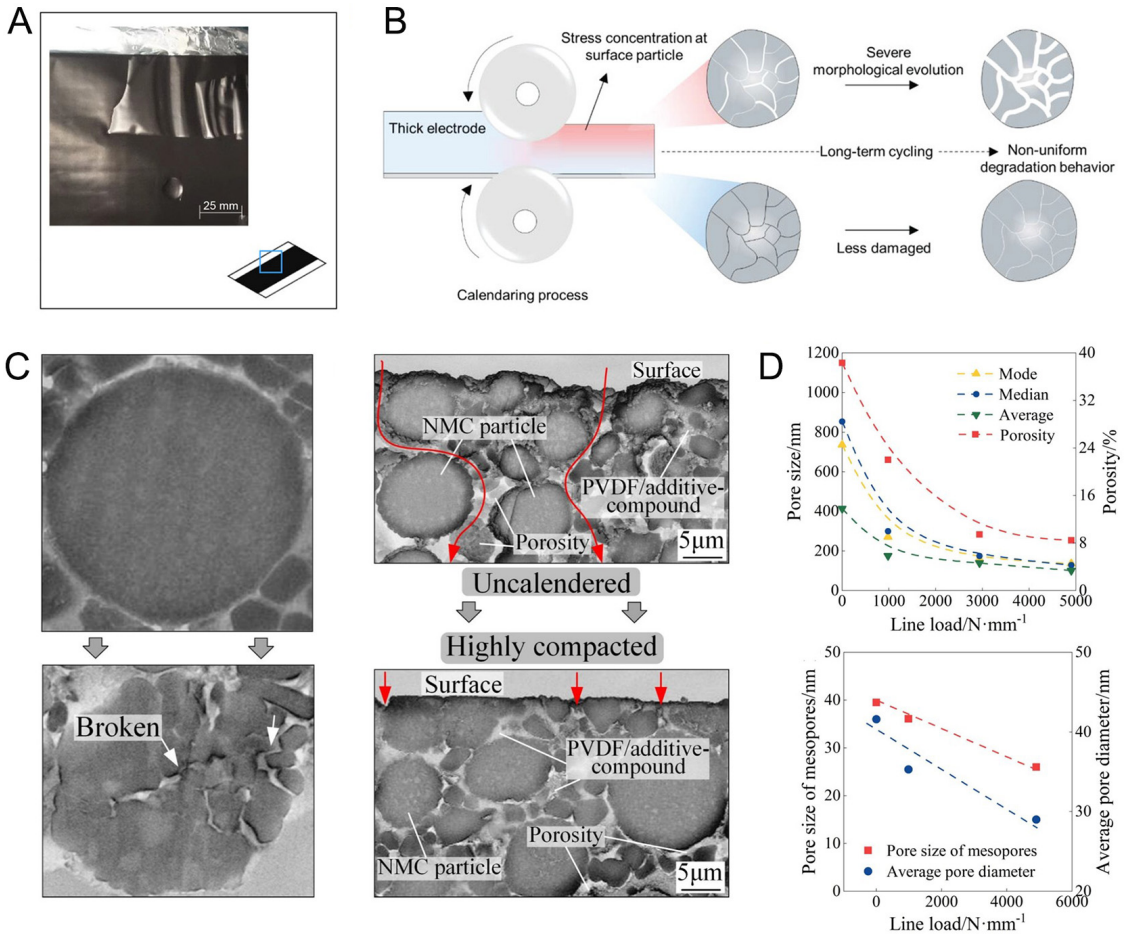


**Figure 6.** Emerged issues observed within the electrode after calendering. (A) Electrode defects observed after calendaring. Reproduced with permission[76]. Copyright 2019, Wiley-VCH. (B) Schematic illustration of thick electrode under strong compressive force applied to polycrystalline Ni-based materials. Reproduced with permission[77]. Copyright 2020, Wiley-VCH. (C) SEM images showing morphological evolution of secondary particle (left) and the electrode cross sectional image (right) under harsh calendaring condition. (D) Variation in porosity and pore size of macropores and mesopores in Ni-based materials with respect to line load. Reproduced with permission[78]. Copyright 2024, Elsevier.

Dissolved TMs easily migrated to the anode surface across the electrolyte, participating in solid electrolyte interphase (SEI) reformation or metal deposition[81]. In the case of Ni-based materials under Ni atomic fraction of 70%, Mn-ions have been reported to significantly contribute to thick SEI formation and metallic Li dendrite growth rather than Ni- and Co-ions, inducing rollover failure by crosstalk[82,83]. However, at a higher Ni fraction (> 80%), Ni-ion crossover could emerge as a critical impact on the anode side due to the high concentration of Ni dissolution into the electrolyte by side reaction at the cathode surface. According to Kim *et al.*, dissolved Ni-ions presented catalytic side reactions on the anode surface, leading to the overgrown SEI layer, low coulombic efficiency, and electrochemical reduction of ions [Figure 7B][84]. The high-resolution transmission electron microscopy (HR-TEM) results in Figure 7C revealed the formation of metallic Ni nanoparticles near the SEI layer. Zhang *et al.* reported a crossover behavior in Si anodes where the impact of TM deposition was more pronounced compared to graphite[85]. Higher depth of lithiation at high-voltage (> 4.3 V) significantly reduces the chemical potential of the Si anode, thereby altering surface chemistry. Subsequently, inhomogeneous electrochemical reactions within Si particles cause Li-ion accumulation inside the silicon structure, resulting in capacity loss and increased internal pressure[86,87].

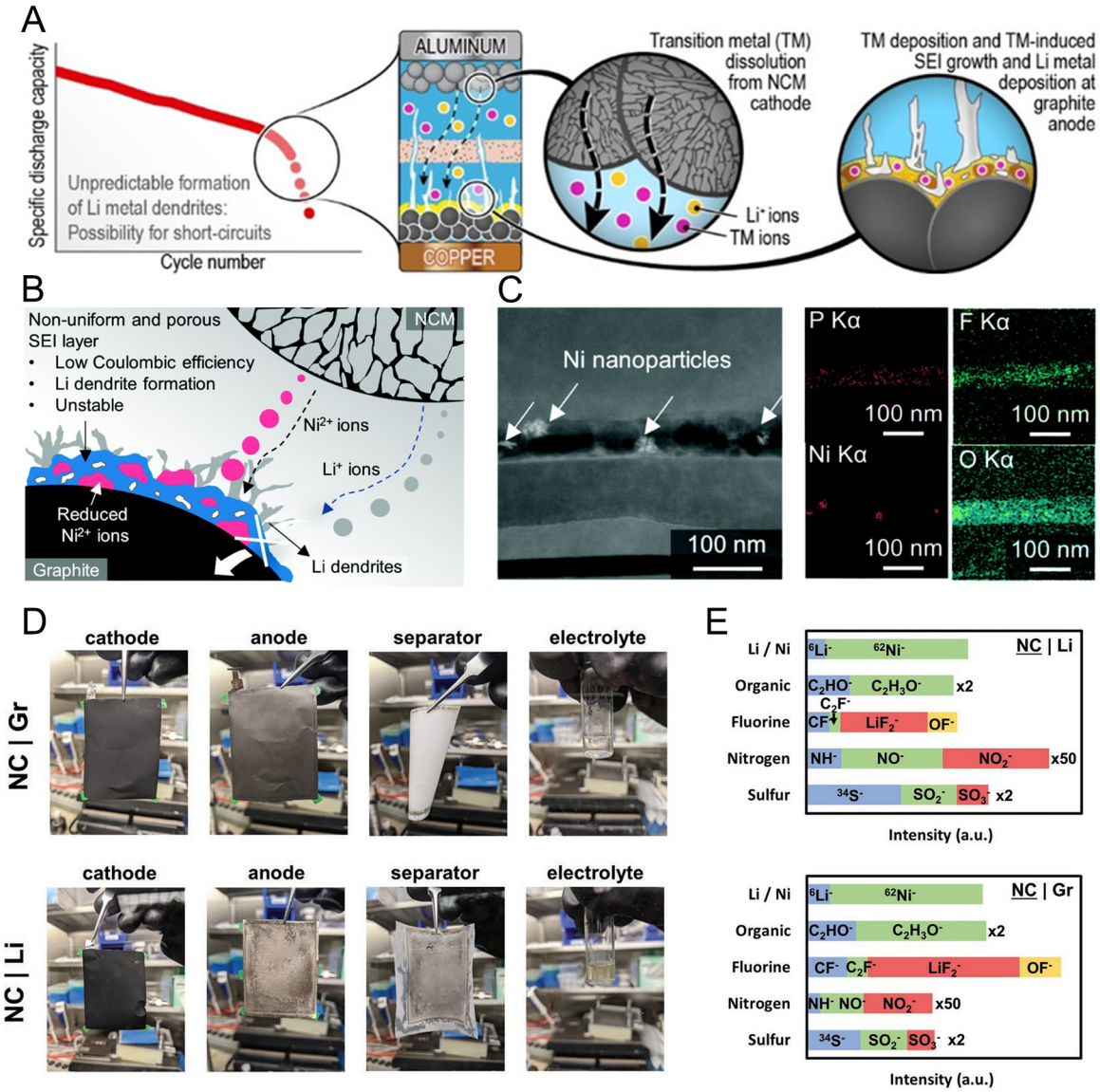


**Figure 7.** Crossover issues of Ni-based materials on diverse anode materials. (A) Illustration of the crosstalk mechanism arising from complex interactions between the anode and cathode. Reproduced with permission[79]. Copyright 2020, Wiley-VCH (B) Crossover impacts of transition metal dissolution from Ni-based materials to the anode side. (C) HR-TEM and EDX mapping images of the graphite anode after full-cell cycling, showing the presence of nickel nanoparticles within the graphite anode. Reproduced with permission[84]. Copyright 2018, Royal Society of Chemistry. (D) Disassembly images of high-Ni cathode pouch cells after cycling, showing cycled electrodes, separator, and electrolyte. (E) TOF-SIMS integrated intensity of various molecular fragments from the cycled high-Ni cathode. Reproduced with permission[91]. Copyright 2022, Wiley-VCH.

In the meantime, utilizing lithium metal anode (LMA) can significantly contribute to capacity fade owing to its high reactivity, such as dendrite growth. In high-mass-loading electrode designs, the uneven distribution of current density and limited ionic conductivity across the thick electrode can promote non-uniform $Li^+$ flux at the anode interface[88,89]. This inhomogeneous plating environment facilitates the nucleation and growth of Li dendrites, particularly under high current densities or during repeated cycling. The formation of Li dendrites induces local current concentration and leads to the accumulation of electrically isolated dead lithium, which contributes to capacity fading during cycling. Langdon *et al.* conducted several studies related to crosstalk on LMAs[90,91]. The findings revealed that high-Ni cathode, paired with LMA, exhibited

much faster capacity loss after 200 cycles compared to cells paired with graphite. Photograph images of cycled cell components in Figure 7D deeply elucidated that LMA induces more reactive side reactions by forming byproducts. Time-of-flight secondary ion mass spectrometry (TOF-SIMS) further demonstrated that lithium metal accelerates cathode degradation and side reactions during cycling based on the intensity of various fragments detected on the cycled cathode [Figure 7E].

## DESIGNING STRATEGIES OF ADVANCED HIGH-NI CATHODES

### Interphase stabilization tailored high-voltage cycling

General strategies for high-Ni cathodes have been mainly focused on the aspect of materials for high-capacitive realization. Unfortunately, higher charge voltage typically expedites side reactions such as electrolyte decomposition and gas evolution, as mentioned in the previous section. Thus, rational CEI has been suggested through electrolyte engineering to suppress detrimental side reactions in high-voltage operations[92,93]. As one of the promising concepts, Xue *et al.* developed a sulfonamide-based electrolyte for the stable design of interphase persisting cathode particle degradation and mitigating side reactions at the cathode/electrolyte interface [Figure 8][19]. The designed electrolyte (1 m LiFSI in *N*,*N*-dimethyltrifluoromethane-sulfonamide (DMTMSA), 1 m LiFSI/DMTMSA) enables stable high-voltage cycling (up to 4.7 V *vs.* $Li/Li^+$) in NCM811 cathodes. Compared to commercial carbonate electrolyte consisting of 1 M $LiPF_6$ in EC and ethyl methyl carbonate (3:7 by weight) with 2 wt% VC (1M $LiPF_6$/EC-EMC + 2% VC), 1 m LiFSI/DMTMSA electrolyte showed stable potential window without gradual electrolyte decomposition at high-voltage, confirmed by linear sweep voltammetry (LSV) analyses [Figure 8B]. Further, this sulfonamide-based electrolyte derived LiF-like inorganic components inside CEIs and thus delayed intergranular stress corrosion cracking (SSC) of cathode particles. Therefore, the designed electrolyte in Li||NCM811 cell enabled stable cycle retention of 88.1% for 100 cycles even under stringent conditions (60 μm Li thickness and 20 μL electrolyte). The stability was verified through various structural analyses. The cathode in designed electrolyte relatively restrained TM dissolution by particle degradation and overgrown CEI, confirmed by inductively coupled plasma mass spectrometry (ICP-MS) measurements while control electrolyte suffered from highly dissolved Ni-ion in the electrolyte after 100 cycles [Figure 8C]. Meanwhile, gas evolution is kinetically accelerated at high voltage due to competitive and side reactions by oxidation decomposition of electrolytes and released oxygen from cathode particles. Typical electrolytes cannot construct stable CEI on the cathode because high-voltage-charging induces unexpected electrochemical and chemical reactions of the electrolyte, interrupting designed electrolyte decomposition. Thus, commercial carbonate electrolyte showed higher gas evolution such as $CO_2$ at the end of charge state (> 4.3 V), measured by *in situ* differential electrochemical mass spectrometry (DEMS) in [Figure 8D, top]. Whereas sulfonamide-based electrolyte enabled to stably construct CEI on the cathode by suppressing side reaction at high voltage and blocking electronic penetration into the intergranular boundary between primary particles, leading to the negligible invoking gas production up to 4.7 V [Figure 8D, bottom]. This behavior consequently prevented the interface between electrolytes and electrodes from additional electrolyte penetration and side reactions that persisted in the cycle life. Therefore, the cathode could suppress SSC degradation and sustain stable secondary particle integration after cycles, while severe cracking was observed in the cathode particle in commercial carbonate electrolyte due to non-uniform electrochemical reaction for individual particles, derived from uneven and overgrown CEI on the electrode [Figure 8E].

In the meantime, ether-based electrolytes have also been explored to apply next-generation batteries using lithium metal as a key anode, stably constructing SEI in the condition of ether solvent[94,95]. However, ether solvent suffered from higher HOMO levels of the solvent molecules, inducing solvent decomposition at lower charge voltage[96,97]. Thus, the compatibility has been concerned in the combination of LMA and high-voltage high-Ni cathode. In this point, Mao *et al.* designed an electrolyte with cyano-substitution ether,

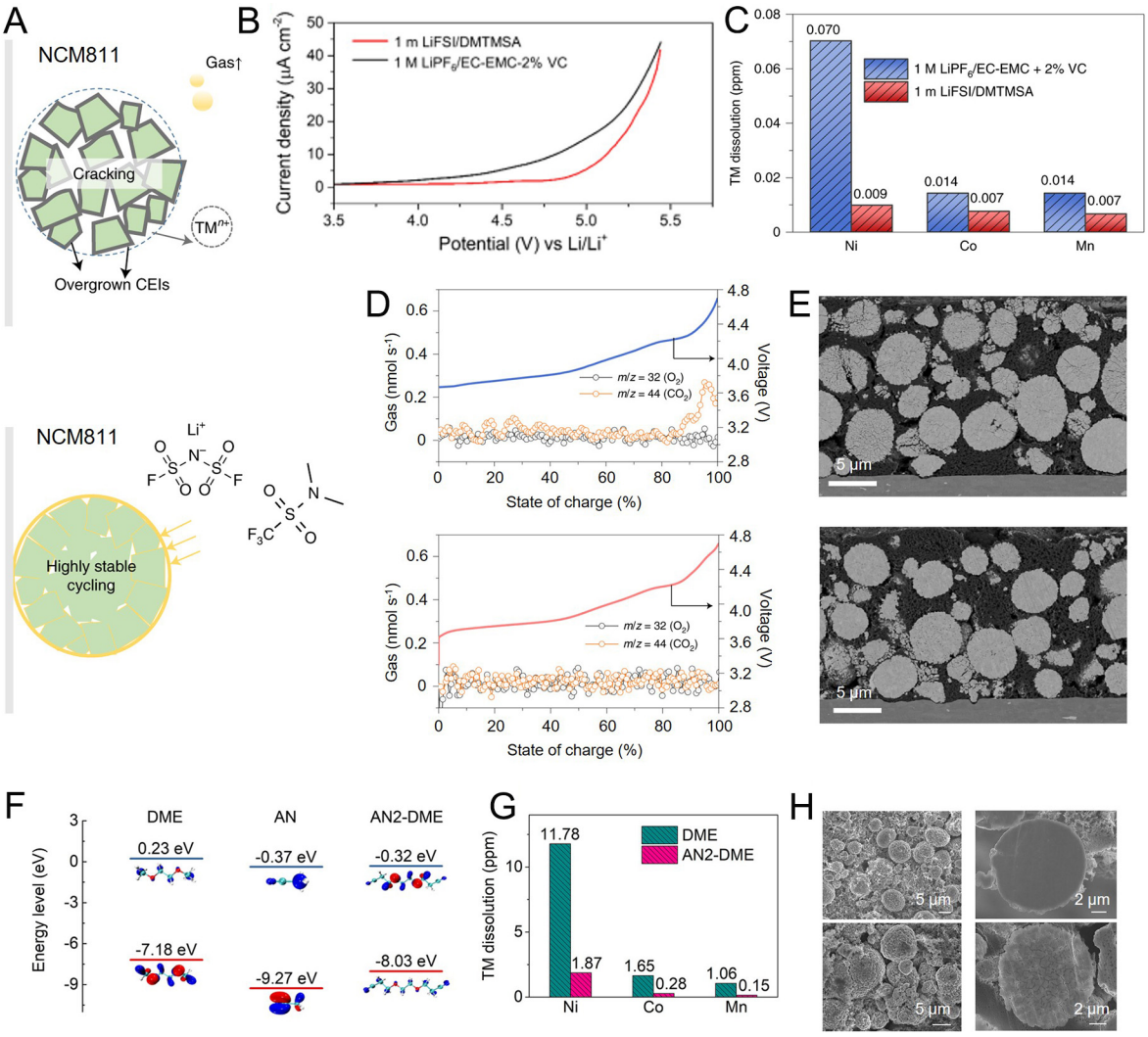


**Figure 8.** Stabilizing interphase for high-voltage realization through electrolyte engineering. (A) Challenges for durable high-voltage Li||NMC811 cells. (B) Electrochemical stability of DMTMSA solvent. (C) TM dissolution measured by ICP-MS after 100 cycles in different electrolytes. (D) *In situ* DEMS analysis in half cells to monitor the gas evolution during first charging in 1 M LiPF6/EC-EMC + 2% VC (left) and 1 m LiFSI/DMTMSA electrolytes (right). (E) cross-sectional SEM images for NMC811 cathodes cycled in 1 M LiPF$_6$ /EC-EMC + 2% VC (left) and 1 m LiFSI/DMTMSA electrolytes (right). Reproduced with permission[19]. Copyright 2021, Springer Nature. (F) HOMO and LUMO of DME, AN, and AN2-DME. (G) TM dissolution measured by ICP-MS after 200 cycles. (H) SEM, and FIB-SEM images of NCM811 particles cycled in AN2-DME-(top) and DME-(bottom) based electrolyte. Reproduced with permission[98]. Copyright 2024, National Academy of Sciences.

ethylene glycol bis(propionitrile) ether solvent (AN2-DME), enabling the enhanced oxidative stability of intrinsic ether solvent by restraining the loss of lone-pair electrons of ether oxygen owing to strong electron-withdrawing cyano-group in the chemical structure[98]. As mentioned, typical ether solvent, 1,2-dimethoxyethane (DME), showed narrow potential window with vulnerable electrolyte stability at high-voltage cycling [Figure 8F]. By contrast, acetonitrile (AN) has a relatively lower HOMO level of molecules which leads the AN2-DME molecule - containing cyano groups in its chemical structure - to intrinsically exhibit a reduced HOMO level and enhanced resistance to oxidative decomposition compared to DME. Further, electron-clouded oxygen located in the ether of AN2-DME could donate electrons to cyanogen, raising the LUMO level, compared to sole AN, compensating SEI stabilization. AN2-DME designed an efficient and stable interphase structure on the cathode at high voltage (> 4.3 V) while sheltering solvent

molecules, hardly influenced by oxidative decomposition, compared to typical DME molecules. Therefore, the electrolyte including AN2-DME solvent showed highly persisting CEI structure even with the potential range of 3.0 and 4.3 V (*vs.* $Li/Li^+$) while achieving the capacity retention of 81.8% for 200 cycles. The evidence was clearly unveiled through much lower TM dissolution, derived from cathode degradation and unstable CEI coverage [Figure 8G]. Besides, the morphological structure of cathode particles, cycled in AN2-DME-based electrolyte, verified that stable interphase led to the restraint of side reaction by unexpected electrolyte penetration and localized intergranular SSC during cycling while DME-based electrolyte cannot preserve the original structure of cathode particle, accelerating the formation of microcrack inside secondary particles [Figure 8H]. The satisfaction of both high-capacitive and high-voltage features should be required in high-Ni cathodes to ultimately realize high-energy-density batteries. In this regard, electrolyte engineering by controlling the chemical structure of solvent molecules could facilitate high-voltage cycling without chronic side reactions, chemically and electrochemically manifested at elevated charge potential.

### Building high-loaded electrodes

Beyond material developments for high-Ni cathodes, the design factor in electrode level should be considered to effectively increase energy/power density because other components, excluding active materials, occupy quite a high weight portion when building practical cells[99]. Thus, the effort to reduce unessential parts has been tried in industry and, as one of key strategies, the electrode has been thickened where the portion of current collectors and separator could be curtailed while increasing main portion to realize the capacity. However, the electrode cannot proportionally increase areal capacity and energy density by simply increasing its thickness. Unfortunately, the difference of molar density, affinity, and surface energy between three components (active, binder, conductive materials) in the electrode slurry. Therefore, the electrode results in uneven distribution of the binder in the electrode by CBD migration during electrode dry process[66,100]. Therefore, wet process for electrode fabrication using the slurry should solve the poor electrode integration. In this regard, Kim *et al.* designed a cationic semi-interpenetrating polymer network (c-IPN) binder to realize uniform charge transfer with structural stability through the control charge-driven electrostatic repulsion [Figure 9A][101]. The regulation of the electrostatic phenomena in slurry-cast electrode fabrication process enabled facile utilization of active materials while facilitating higher areal capacity (C/A) cathode design. This approach could reduce both cell thickness and weight, compared to typical low C/A cathode. In practice, the electrode using c-IPN binder showed the areal mass loading (M/A) of 96 mg $cm^{-2}$ with significantly even particle distribution according to elemental mapping results of Ni and carbon (C) in the electrode [Figure 9B]. As mentioned, normal electrodes using conventional binders cannot proportionally increase the areal capacity as a function of mass loading due to poor electrode integrity. By contrast, c-IPN applied electrode showed steady increase of areal capacity as the mass loading was raised, guaranteeing superior structural and electrochemical integrity [Figure 9C]. Charge regulation of cationic binder also enabled facile Li-ion mobility in whole electrode by trapping anion in the electrolyte [Figure 9D].

Meantime, slurry-based electrode fabrication has been modified through structuring architecture to realize high-mass-loading and thick battery electrode. Kim *et al.* demonstrated a unique strategy based on a bicontinuous electron/ion conduction network-embedded quasi-solid-state (BNQS), as illustrated in Figure 10A[102]. Electroconductive-mat layers consisting of single-walled carbon nanotubes (SWCNT) had a role of support framework to conduct repetitive electrode stacking through slurry cast and finally produce high-mass-loading and thick electrodes (60 mg $cm^{-2}$ and 315 μm) without electrode cracking or delamination. Further, gel electrolyte-based precursor assisted unit electrode layers to design uniform and homogeneous internetwork and besides after ultraviolet (UV) curing, the unit electrode showed sturdy mechanical and chemical stability to enable stacking the electroconductive-mat layer and additional unit

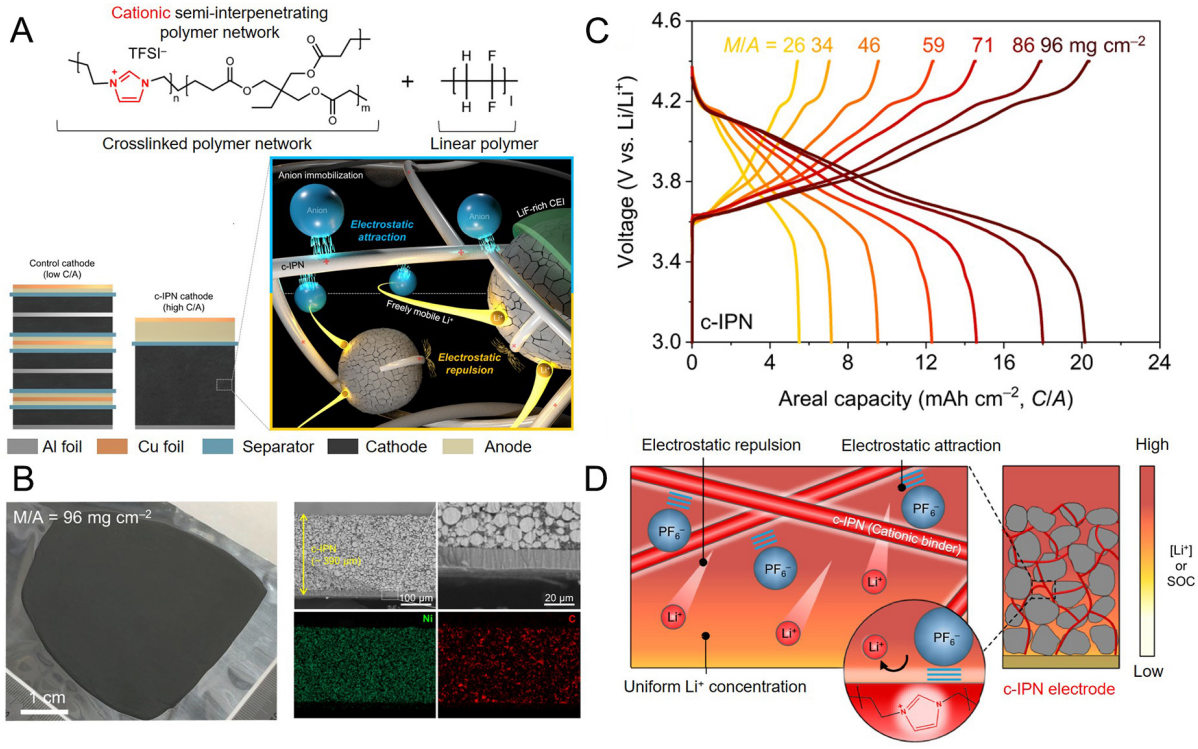


**Figure 9.** High-energy-density realization through slurry-based electrode fabrication. (A) Schematic illustration showing the superiority of the c-IPN cathode. (B) Photograph and cross-sectional SEM with EDS images of the c-IPN electrode. (C) Galvanostatic charge/discharge profiles of the cells as a function of the M/A of the cathodes at 25 °C. (D) Schematic illustration showing the role of the c-IPN binder. Reproduced with permission[101]. Copyright 2023, Springer Nature.

electrodes without the architecture destruction. Whereas, as mentioned, one-pot slurry casting to build high-mass-loading and thick electrodes inevitably induces chronic issues related to CBD migration and localized extinct charge networks. In this regard, BNQS verified a stable carbon distribution and electrochemical integrity in whole electrode that the 3D microstructural analysis through focused ion beam (FIB) nanotomography and 3D reconstruction process showed uniform carbon (yellow) distribution [Figure 10B]. This result indicates that conductive agents were well-dispersive in each unit electrode between electroconductive-mat layer without remarkable migration during electrode fabrication process. Besides, cross-sectional SEM images displayed a dense and uniform distribution of electrode ingredients in the direction of thickness where electroconductive-mat layers stably supported each unit electrode in BNQS [Figure 10C, left]. In terms of charge interconnection, the mapping image for localized charge transfer resistance guaranteed a homogenous electrochemical network and low resistance in whole electrode without isolated NCM811 particles [Figure 10C, right]. Post-mortem analyses after cycling further supported advances of BNQS with well-designed electrode architecture. Typically, high-Ni cathodes such as NCM811 suffered from TM dissolution and surface deformation due to structural degradation during cycling. For this reason, the virgin NCM811 cathode showed a layered structure transition to rock salt structure at the surface and nickel fluoride ($NiF_2$) formation by unexpected electrochemical reaction with the electrolyte. Thus, the one-pot slurry-cast NCM811 cathode inevitably led to the generation of high-concentrated NiF2 at the cathode surface after cycling [Figure 10D]. Uneven electrochemical reactions and high charge transfer resistance in the electrode by poor carbon dispersion induced the deviation of charge depth in NCM811 particles and finally resulted in severe side reactions. By contrast, in BNQS, cured gel polymer structure strongly interacted with each NCM811 particle between electrolyte and electrode by stable interphase formation in advance. Therefore, the surface of BNQS showed much lower concentration

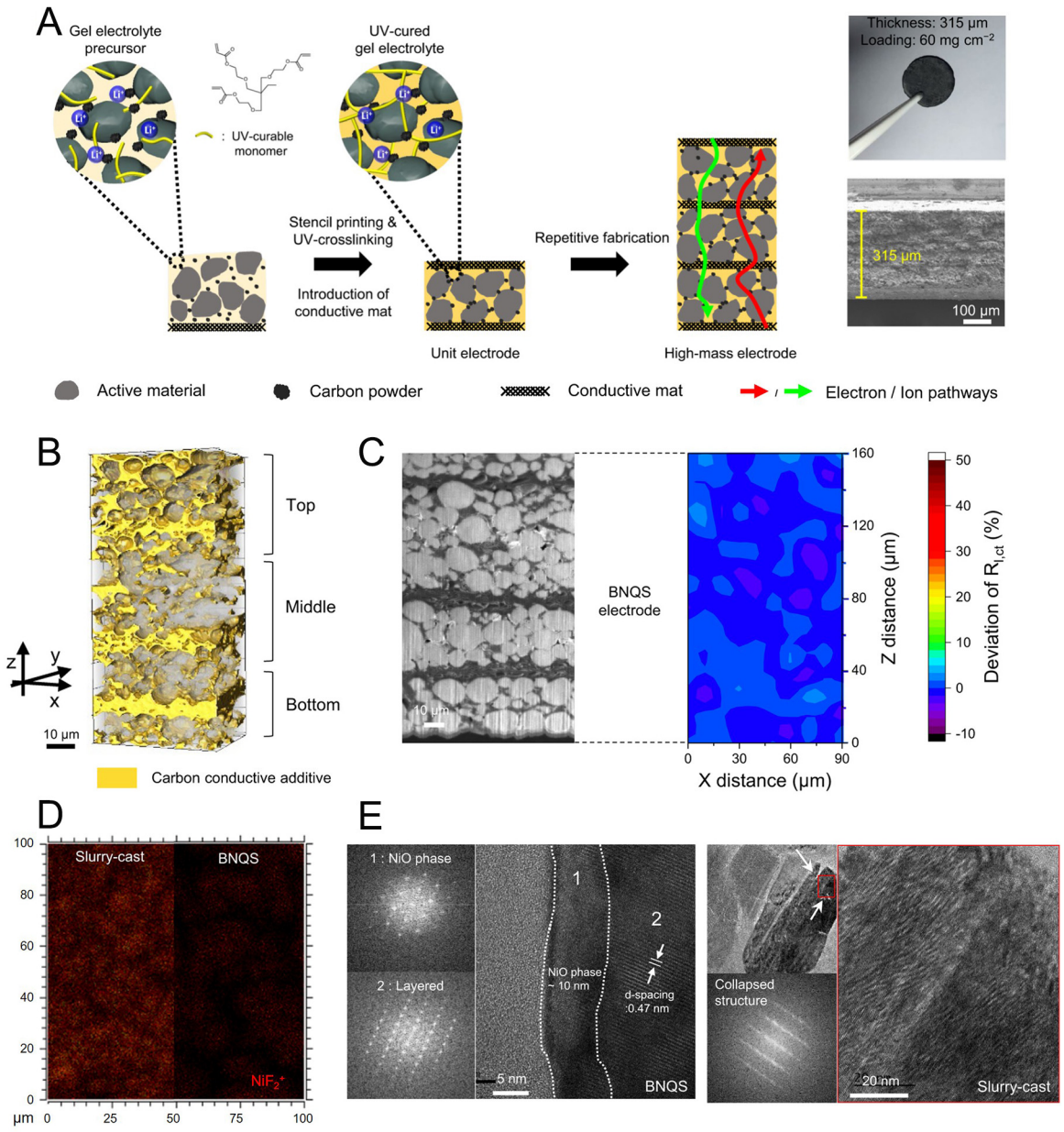


**Figure 10.** High-energy-density realization through slurry-based electrode fabrication. (A) Schematic representation of the structural design and fabrication procedure of high-mass-loading BNQS electrode, along with its photograph and cross-sectional SEM image. (B) 3D microstructural analysis, focusing on carbon (colored in yellow) distribution of BNQS electrodes. (C) cross-sectional SEM images (left), corresponding localized charge transfer resistance (Rl,ct) obtained from LEIS analysis (right) of BNQS electrodes. (D) TOF-SIMS mapping images of the $NiF^{2+}$ byproducts formed on the surface of the cathodes. (E) HR-TEM images with fast Fourier transform patterns of the NCM811 particles of slurry-cast and BNQS cathodes. Reproduced with permission[102]. Copyright 2022, Springer Nature.

of $NiF_2$ after cycling because the well-designed interphase effectively suppressed TM dissolution and side reaction. Besides, HR-TEM additionally verified that BNQS maintained its original layered structure with thin surface degradation into rock salt structure while the one-pot slurry-cast electrode showed structural destruction by severe side reaction and unexpected byproduct formation [Figure 10E]. Consequently, high-loaded and thick cathode fabrication could become a game changer to realize ultimate high-energy-density batteries beyond rationally designing high-Ni cathode materials. At this point, the aforementioned strategies

use a functional binder and stable architecture to maintain the slurry casting process.

In the meantime, with the critical issue of climate change and carbon neutralization, another electrode fabrication process should be developed, excluding the generation of volatile organic compounds (VOCs) and reducing the footprint in the electrode manufacturing system[17,103]. In this regard, an innovative electrode manufacturing concept, dry electrode, has been suggested to solve emerging issues. Yao *et al.* facilitated the dry electrode fabrication process of the LNMO cathode through the fibrillation of a polytetrafluoroethylene (PTFE) binder[104]. Typical slurry-based process requires continuous drying process after slurry casting and vacuum drying at the end of electrode coating process involving toxic vapor of solvent, as illustrated in Figure 11A[104]. Further, the slurry-based system needs additional footprint for solvent recovery tank to reuse solvents, applied in slurry mixing step for the reduction of operational expenditure. In an aspect of electrode quality, the slurry-based processes cannot clearly design high-loaded and thick electrodes at a practical level, intrinsically leading to heterogeneous distribution and local cracking in the electrode. By contrast, dry electrode manufacturing process enables cost-down of manufacturing process and saving of energy consumption owing to solvent-free system, not requiring solvent in whole process. Therefore, general process of dry electrode consisted of dry powder mixing, shearing (mixing/kneading), film formation, roll press (calendering), and lamination process without any solvent-drying process. Besides, the solvent-free system does not experience electrode shrinkage and CBD migration, derived from the drying process in slurry-cast electrode, and thus, the dry process enables the construction of a crack-free electrode. Therefore, the dry-coated cathode showed well-distributed active materials in the whole electrode structure, constructed with an areal capacity of 9.5 mAh $cm^{-2}$ and a thickness of 240 μm [Figure 11B, left]. In contrast, slurry-coated cathode resulted in aggregated carbon cluster by CBD migration on drying solvent despite relatively thin electrode formation with the areal capacity of 4 mAh $cm^{-2}$ and a thickness of 110 μm [Figure 11B, right]. Moreover, as mentioned, the uniformity of electrode ingredients directly influenced electrochemical stability at the electrode level. A well-dispersed conductive agent throughout the electrode enables even spreading of charge carriers, leading to stable current flow and a uniform state of lithiation. In this regard, the dry-coated cathode showed higher and more uniform current flow throughout the electrode, as observed via a 2D modeling process [Figure 11C, left]. Therefore, the dry-coated cathode exhibited a clear delithiation process for individual active materials at the end of the discharge state. In contrast, some active materials in the slurry-based cathode remained lithiated even after the full discharge process due to poor electrochemical integrity in the electrode [Figure 11C, right]. Besides, the electrode requires high mechanical endurance to ensure a stable electrode and cell fabrication process because additional engineering challenges have emerged in high-mass-loading and thick electrodes, such as CBD migration and particle isolation. In this regard, homogeneous electrode design is also important to achieve crack-free and stable integration during the dry process. Thus, to further confirm electrode strength, the peel-off tests were conducted depending on electrode fabrication process. As summarized in Figure 11D, the slurry-based cathode showed weak electrode integrity and low binder dispersibility according to easy electrode delamination under lower peel-off force. On the other hand, the cathode, fabricated through dry process, featured higher mechanical strength in the electrode while exhibiting stable endurance under relatively higher peel-off force. As a result, the dry cathode, which enables uniform distribution of each electrode ingredient without localized aggregation, can facilitate both electrochemical and structural stability and has the potential to realize high-energy-density batteries by allowing increased mass loading and electrode thickness.

Meanwhile, the electrode integrity could be decided through roll press (calendering) process, going beyond the simple mixing process. Dry electrodes are typically fabricated as free-standing films without a current collector, unlike slurry-based electrodes. Further, higher pressure should be required to obtain expected

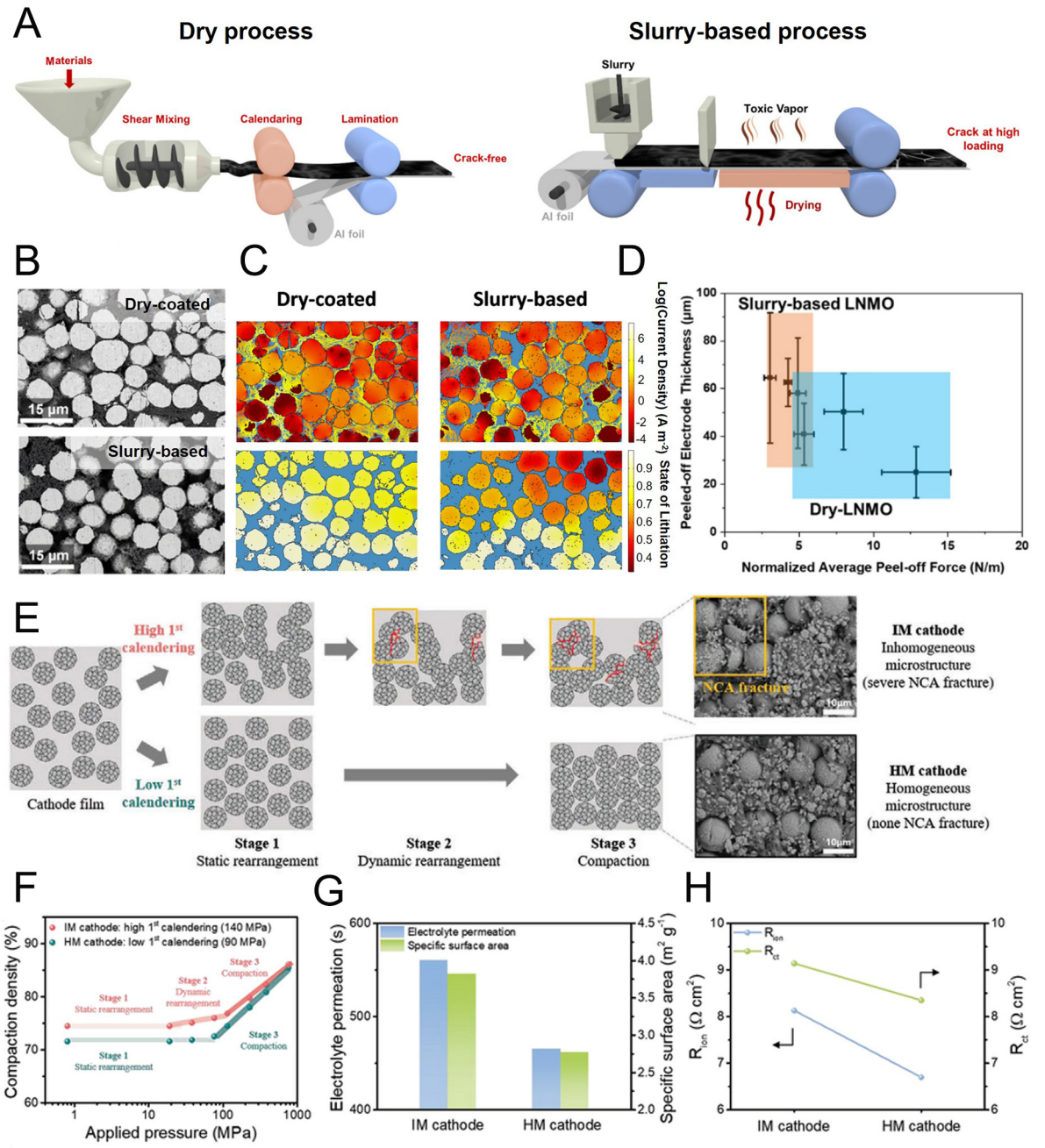


**Figure 11.** High-energy-density realization through dry electrode fabrication. (A) Schematic of dry electrode and slurry-based cathode fabrication procedures. (B) Plasma focused ion beam (PFIB)-SEM cross-sections of dry coated (left) and slurry-based LNMO (right). (C) 2D modeling results at the end of a discharge at C/3 are displayed with the current density in the solid phase and the state of lithiation reported for the dry coated LNMO (left) and for the slurry-based LNMO (right). (D) Normalized peel-off forces and thickness of peeled-off electrodes from both dry-LNMO and slurry-based LNMO at an areal loading of 3.0 mA h $cm^{-2}$. Reproduced with permission[104]. Copyright 2023, The Royal Society of Chemistry. (E) Schematic illustration and SEM images of dry electrode depending on 1st pressure during the calendering process. (F) Compaction diagram for the IM and HM cathodes. (G) Specific surface area and electrolyte permeation and (H) $R_{ion}$ and $R_{ct}$ for the IM and HM cathodes, respectively. Reproduced with permission[105]. Copyright 2024, Wiley-VCH.

composite density of electrode owing to higher thickness. In this regard, Kim *et al.* deeply considered optimal roll press process, focusing on microstructure evolution to design rational electrode structure[105].

Direct application of high pressure to the free-standing film can cause unexpected electrode degradation due to mechanical damage such as cracking and pulverization of polycrystalline NCA particles. Therefore, the roll press process should be carefully controlled and optimized for suitably thick dry electrode films to successfully complete the electrode fabrication process. At this point, the two-step pressing process was suggested [Figure 11E]. Relatively lower pressure (90 MPa) in 1st pressing could lead to the rearrangement behavior of NCA particles and homogeneous microstructure (HM) cathode with the uniform packing of electrode film and no particle fracture. By contrast, higher pressure (140 MPa), applied to the electrode film as 1st pressing step showed particle pulverization because the film hardly provided relaxation time to move the NCA particles into free volume in the film, inducing severe fracture of NCA particles and inhomogeneous microstructure (IM) formation. In the experiment, when the compaction density of electrode film was measured as the function of applied pressure as shown in Figure 11F, the HM cathode can endure film structure without remarkable increase of compaction density by particle rearrangement while the IM cathode inevitably showed gradual increase of the density by continuous collision of particles and structure destruction during film pressing showing different packing behavior. This phenomenon additionally influenced electrolyte permeability into the thick electrode. Robust particle rearrangement in HM cathode through mild pressing step enabled uniform particle and pore structure evolution and thus HM cathode resulted in short time for electrolyte permeation even though the cathode featured lower surface area by the maintenance of secondary NCA particles [Figure 11G]. This structural enhancement was connected to electrochemical kinetics where HM cathode showed lower electrochemical resistance in aspect of both ion migration charge transfer [Figure 11H]. Consequently, engineering manipulation through fabrication processing of dry electrode should be deeply understanded to utilize stable high-mass-loading and thick electrode without mechanical/electrochemical loss. From the electrode perspective, higher areal capacity of high-Ni cathodes was an important design factor, and electrodes could be designed with higher mass loading and thickness by controlling the electrode manufacturing process.

### Compatible electrolyte design with various anodes

Compatibility with various anodes at the cell level should be considered alongside cathode development. In this context, electrolyte compositions have been explored depending on the anode type to address the aforementioned crossover issues. High-voltage cycling inevitably showed capacity degradation due to electrolyte oxidative decomposition and structural destruction of the cathode. At the cell level, the behavior was accelerated by the additional side reaction on the anode, derived from cathode degradation, finally inducing crosstalk and "rollover" failure at high-voltage cycling[106,107]. Dissolved TM ions were deposited on the anode as the form of metal fluorides. This issue subsequentially induces uneven electrochemical reaction and high overpotential of graphite and finally resulted in cell failure by dendritic growth of lithium metal on the graphite anode. In this regard, Klein *et al.* suggested new electrolyte concept, EC-free electrolyte composition, and powerful additive in carbonate-based electrolyte[108]. Typical electrolytes containing EC solvent, 1.0 M $LiPF_6$ in EC/EMC (3/7, w/w) obviously suffered from "rollover" failure by TM dissolution and the growth of Li dendrite [Figure 12A]. By contrast, EC-free electrolytes, only including EMC solvent, showed stable cycle retention for 100 cycles without sudden capacity decay. Figure 12B clearly verified that the EC-free electrolyte led to the suppression of TM dissolution from the cathode, showing no remarkable TM deposition on the graphite anode, while the EC-containing electrolyte had an uneven surface of the anode surface, including deposited TM compounds. Meantime, the additive, lithium difluorophosphate ($LiPO_2F_2$, LiDFP) also prevented "rollover" failure of full cell even under EC-containing electrolyte for 100 cycles [Figure 12C]. Comprehensively, the effect can be sufficiently elucidated through the TM scavenging ability of $PO_3F$-based species, one of $Li_xPO_yF_z$ series in the electrolyte, derived from $LiPF_6$ decomposition or LiDFP additive. As shown in Figure 12D, $PO_3F_2$-ions featured the reduction of TM ion concentration as the role of a TM scavenger where the ions successfully verified chemical interaction with TM-ions in the solution gradually reducing the ion concentration. This anion could be generally produced by

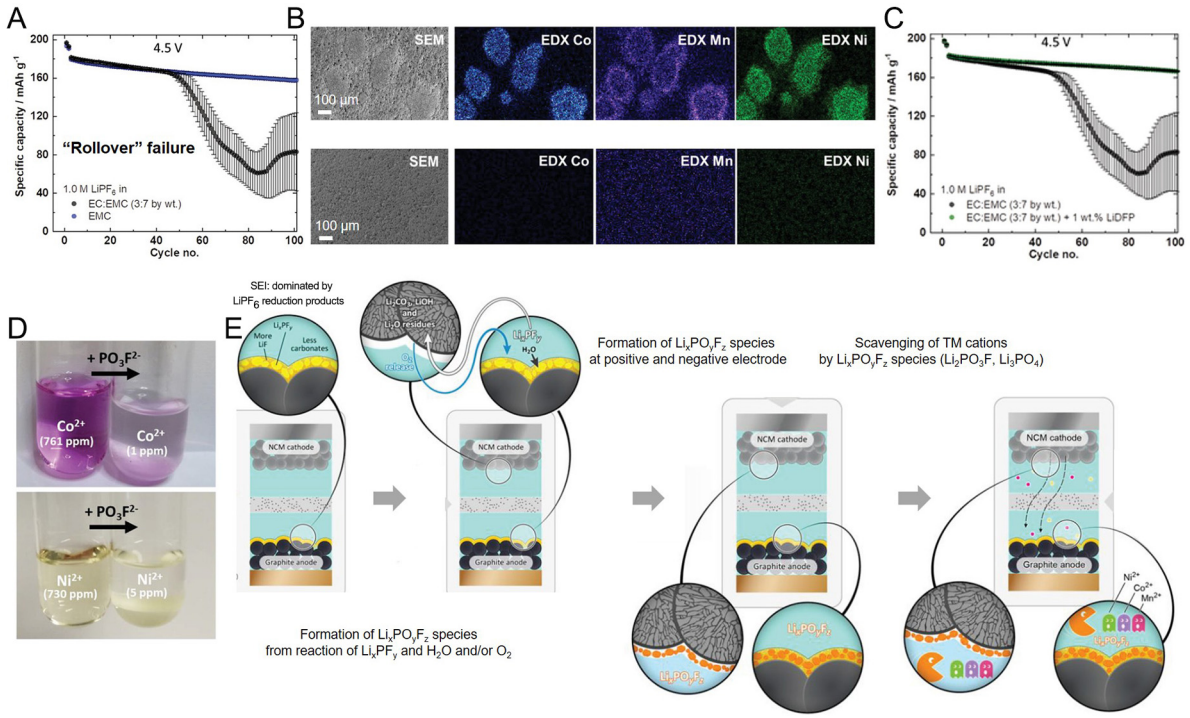


**Figure 12.** Compatible electrolyte design with anode; graphite. (A) Charge/discharge cycling of NCM523||graphite full-cells (2.8-4.5 V) for EC-free electrolyte. (B) SEM-EDS images of graphite-based anodes after 100 charge/discharge cycles with EC-based (top) and EC-free electrolytes (bottom). (C) Charge/discharge cycling of NCM523||graphite full-cells (2.8-4.5 V) with the addition of 1 wt% LiDFP in EC-based electrolyte (C). (D) Precipitation experiments: the addition of an exemplary $PO_3F^{2-}$-based species to $Ni^{2+}$- and $Co^{2+}$-containing EC-based electrolyte significantly reduces the transition metal ion concentration. (E) Mechanism of the rollover fading suppression of the EC-free electrolyte. Reproduced with permission[108]. Copyright 2021, Wiley-VCH.

electrochemical decomposition of $LiPF_6$ at the interface of electrolyte and anode. However, EC solvent preferentially reacted to form an SEI layer on the anode, reducing the participation of $LiPF_6$ decomposition. Therefore, the EC-containing electrolyte cannot protect TM deposition. By contrast, sole EMC solvent in the electrolyte enabled smooth electrochemical decomposition of $LiPF_6$ forming $Li_xPO_yF_z$ on the anode and electrolyte, as illustrated in Figure 12E. Thus, even though TM was inevitably dissolved from cathode, the scavenger can remove unexpected ions in the electrolyte preventing crosstalk and "rollover" failure in advance.

While strategies withstanding high-voltage operation have been developed in graphite anodes, additional missions should be addressed in other anodes with different electrochemical reaction mechanisms that realize high specific capacity, alloying/dealloying (Si) and electrodeposition/dissolution (Li). The electrolyte concept for high-Ni cathodes paired with Si or Li-based anodes focuses on forming a sturdy and functional interphase layer on each electrode. Thus, the electrolyte can be selected to perform positive roles in both oxidative and reductive decomposition on the cathode and anode, respectively. In this regard, as an example, Park *et al.* designed the composition of functional additives, 5-methyl-4-((trifluoromethoxy)methyl)-1,3-dioxol-2-one (DMVC-$OCF_3$) and 5-methyl-4-((trimethylsilyloxy)methyl)-1,3-dioxol-2-one (DMVC-OTMS) with VC and fluoroethylene carbonate (FEC) in carbonate-based electrolyte[109]. DMVS-$OCF_3$ initiated electrochemical reduction for SEI formation on the Si-C anode and then $OCF_3$ anion sequentially produced lithium fluoride (LiF) inorganic compounds enabling to increase mechanical strength of SEI, as illustrated in Figure 13A. Besides, one-electron reduced DMVC-$OCF_3$ and DMVC-OTMS, producing DMVC radicals experienced the polymerization through the interaction of VC

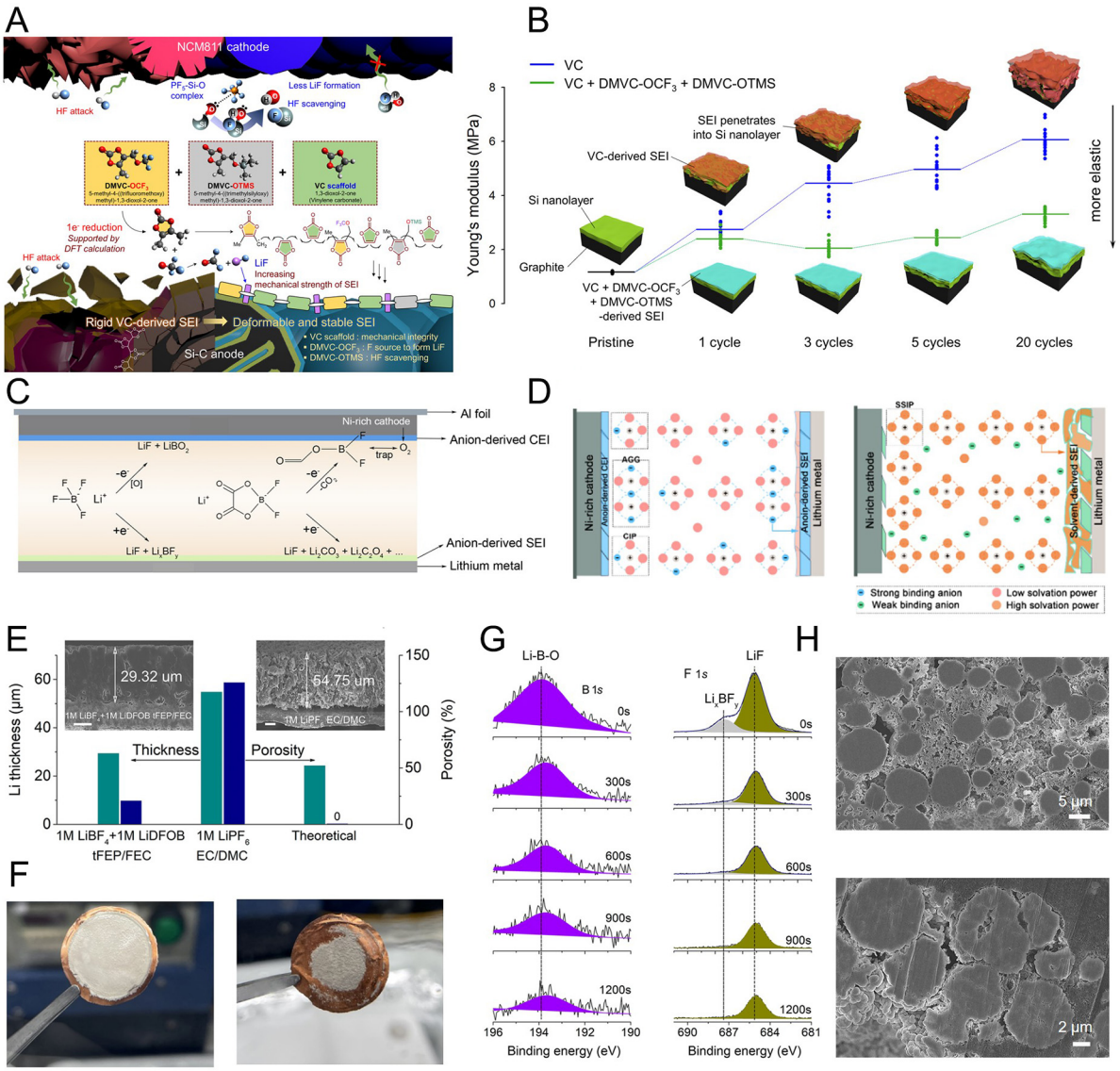


**Figure 13.** Compatible electrolyte design with anode: Silicon/Graphite. (A) Schematic illustration for the incorporation of DMVC-OCF3 and DMVC-OTMS in the VC scaffold leads to the creation of a flexible and robust solid electrolyte interphase (SEI) on the Si-C anode. (B) Tendency of the Young's modulus of the Si nanolayer of the Si-C anode during cycling of NCM811/Si-C full cells. Reproduced with permission[109]. Copyright 2021, Springer Nature. Li metal. (C) Schematic illustration of anion-enrichment interface and anion-derived interphases. (D) Schematic illustration of anion-rich solvation structure and anion-derived interphase (left) and conventional solvation structure and solvent-derived interphase (right). (E) Electrode thickness and porosity of deposited Li calculated from focused ion beam-scanning electron microscopy (FIB-SEM) results. Inset are cross-section SEM images of Li metal deposited on Cu at the current density of 0.5 mA $cm^{-2}$ for 10 h. Scale bar: 10 μm. (F) Digital images of Li deposited on Cu foil and corresponding separators in 1M $LiBF_4$ + 1M LiDFOB tFEP/FEC (left) and 1M $LiPF_6$ EC/DMC (right). (G) XPS spectra of B 1s and F 1s for LMA in 1 M $LiBF_4$ + 1 M LiDFOB tFEP/FEC electrolyte. (H) SEM images of cross-sectioned NMC811 cathodes cycled in 1 M $LiBF_4$ + 1 M LiDFOB tFEP/FEC (top) and 1 M $LiPF_6$/EC-DMC (bottom) electrolytes. Reproduced with permission[110]. Copyright 2023, Springer Nature.

additive constructing VC scaffold affecting mechanical integration of formed SEI by designed electrolyte. With this electrochemical behavior, Si-C could build a sturdy interphase layer to endure mechanical strength against volume change of Si particles and raise ionic conductivity by LiF, derived from DMVS-$OCF_3$. With the structural assistance for enhanced SEI and CEI layers, the full cell showed stable cycle persistence for 400 cycles with steady overpotential observation. The electrolyte with functional additives,

DMVC-$OCF_3$ and DMVC-OTMS, showed elastic manipulation of Si-C anode structure while modulating electrode stress against volume expansion while featuring lower Young's modulus during cycling [Figure 13B]. It means well-combined additive molecules in the electrolyte effectively built a stable SEI layer and smoothly managed interphase integrity, beneficial for enduring the volumetric stress. In the meantime, functional additives positively influenced the CEI layer on the cathode. While constructing stable SEI one the anode, typical FEC is used as essential additive to design LiF-rich interphase in Si-based anode and $LiPF_6$ salts generate LiF and $PF_5$ by product under electrochemical reaction. Unfortunately, $PF_5$ structure induces the defluorination of FEC leading to unexpected HF byproducts and gas evolution to degrade as-formed CEI. At this point, DMVC-OTMS plays a critical role in suppressing HF and gas generation by deactivating the $PF_5$ side reaction through bond interactions that form a $PF_5$-Si-O complex in the electrolyte. SEI and CEI layers further maintained the structural stability because DMVC-OTMS could scavenge HF molecule, which destroyed the interphase layer and subsequently induced consecutive electrolyte decomposition to repair damaged SEI and CEI layers. Consequently, compatible electrolyte composition with dual-functional additives simultaneously stabilized both anode and cathode interphases to facilitate the configuration of high-Ni cathode with high-capacitive anode system for high-energy-density batteries.

Cycle stability of the cell configuration of high-Ni cathode and LMA could also be realized through electrolyte modification tailoring both cathode and anode. As one of rational electrolyte concepts, Mao *et al.* designed fluorinated linear carboxylic ester (ethyl 3,3,3-trifluoropropanoate, tFEP)-based electrolyte with two kinds of lithium salts (lithium tetrafluoroborate, LiBF4 and Lithium difluoro(oxalato)borate, LiDFOB) to prepare weakly solvating and dissociated electrolyte (WSDE) to form abundant contact ion pairs (CIP) and aggregates (AGG) with decoupling the interaction between Li-ion and solvents [Figure 13C][110]. This electrolyte system could make high amounts of anions occupied at the electrolyte interface and anion-enriched SEI and CEI layer preferentially including large amounts of LiF and lithium borate inorganic molecules by chemical structure of adopted salts [Figure 13D, left][111,112]. By contrast, conventional electrolyte featured solvent separated ion pair (SSIP)-dominant structure leading to solvent-derived SEI and poorly protected CEI layer due to hardly any positive ingredients experiencing oxidative decomposition on the cathode [Figure 13D, right]. With anion-enriched SEI layer, lithium metal, electrodeposited in designed electrolyte with dual salt in ester-based solvent, showed dense and stable morphological formation while conventional electrolyte inducing solvent-derived SEI showed dendritic growth, resulting in fast capacity decay and safety issues by short-circuit [Figure 13E][113,114]. Besides, photograph images of electrodeposited lithium metal on copper (Cu) foil verified anion-enriched SEI layer by CIP and AGG structure facilitated even ionic flux and 2D diffusion kinetics for the metal electrodeposition [Figure 13F, left]. In contrast, SSIP solvation structure in conventional electrolyte induced inhomogeneous electrochemical reaction and non-uniform lithium metal deposition on the current collector because as-form SEI cannot utilize higher ionic and mechanical enhancement [Figure 13F, right]. In-depth X-ray Photoelectron Spectroscopy (XPS) analyses of anion-enriched SEI layer further guaranteed lithium borate-rich and LiF-rich interphase enabled stable lithium metal formation without dendritic growth [Figure 13G]. Meanwhile, the critical solvation structure in ester-based electrolytes also influenced the formation of an anion-derived CEI layer, promoting preferential oxidation decomposition of Li salts instead of solvent participation. This behavior could suppress gas evolution during high-voltage cycling (> 4.6 V) and protect against TM dissolution and microstructural degradation of the high-Ni cathode. Furthermore, stable LMA during cycling supported structural stability by controlling electrochemical overpotential. Therefore, as well as on the anode side, the designed electrolyte composition positively contributes to the persistence of cathode stability, showing no remarkable intergranular SSC during cycling, whereas conventional electrolytes suffered from microcracking within the particle structure [Figure 13H].

As described, both the cathode and anode must be considered to ultimately realize stable high-Ni cathode-based high-energy-density batteries. In this regard, compatible electrolytes tailored for both the cathode and various anodes have been introduced, and the electrochemical behavior of the designed electrolytes during electrochemical reactions has been thoroughly investigated. Beyond simple materials design of the high-Ni cathode, a comprehensive perspective at the electrode and cell level is essential to practically apply advanced high-Ni cathodes in desirable battery systems with high stability and energy density.

## CONCLUSION AND SUMMARY

High-Ni cathodes have attracted attention to increase specific capacity for high-energy-density batteries and have been refined at the material level. Unfortunately, applying these materials causes severe side reactions and structural degradation during cycling compared to conventional cathode materials. However, the sole material cannot effectively improve battery performance in practical applications because typical cells should consider emerging issues interacting with the electrolyte and anode. Thus, high-Ni cathodes have been complexly explored for unveiled issues, and we summarized strategic approaches at the electrode level, such as electrode design and electrolyte engineering, for high-energy-density and stable batteries. These suggested approaches developed homogeneous and high-loaded electrode structures through ingredient modification such as binder and substrate architecture in the wet process, while the dry manufacturing process enabled systematic advancements in both fabrication and electrochemical properties. Electrolyte composition was selectively tailored for interphase manipulation, suitable for high-voltage operation and dissolution suppression in cathodes. Besides, in terms of cell configuration, it was investigated with the combination of diverse anodes for practical feasibility.

Therefore, addressing improvements for the cathode requires deep consideration beyond simple material modification, focusing on the electrode level. This necessity arises because a battery constitutes a complex integrated system, comprising not merely the cathode material itself. Other constituents such as the anode and electrolyte are intimately interconnected with the cathode and exert significant influence on one another.

## CHALLENGES AND OUTLOOK

Considerable advances have been reported through various systematic concepts and approaches for high-Ni cathodes, delicately summarized in this review. However, remaining challenges exist to effectively replace existing systems because the battery system should be examined from a comprehensive standpoint that encompasses all its requirements, moving beyond a perspective solely focused on energy density and stability. In particular, in the electrode architecture, the dry battery electrode enables the efficient design of high-loaded and thick structures with HM owing to absence of CBD migration. Further, the smaller footprint by dry-free system derives manufacturing advantages in both capital/operational expenditures. While conventional PTFE binders are widely used in dry electrodes due to their structural advantages, they are required to be replaced due to per- and polyfluoroalkyl substances (PFAS) regulations. Unfortunately, the lack of readily available binder systems to effectively replace PTFE currently presents a challenge from an environmental perspective. Further, the realization of fast charging, which has not been prominently addressed, presents a critical challenge. Thicker electrodes, compared to conventional electrode ones, pose difficulties in achieving high-power-density due to insufficient electrolyte impregnation within the whole electrode. Accordingly, to effectively enable fast-charging in dry electrodes, practical solutions of low viscous electrolytes or modification of the electrode architecture such as gradient and aligned structure are required. Meanwhile, rational electrolyte compositions in advanced high-Ni cathode-included battery systems have significantly improved electrochemical and structural stability. However, from the standpoint of cost competitiveness, electrolyte combinations, as suggested, that barely reflect cost considerations face a

significant barrier, which can become a fatal drawback for system changes at a practical level. Therefore, it is necessary to continuously consider simple and effective electrolyte compositions with competitive salts and additive candidates.

In the near future, the potential of high-Ni cathodes needs to be systematically demonstrated at the cell level and broader perspectives. Ultimately, achieving desired battery configuration and specifications for the electrification of large-scale devices and ESSs will necessitate comprehensive design and engineering by thoroughly addressing various interacting factors.

## DECLARATIONS

### Authors' contributions

Data sourcing, collection, and paper writing-original: Jin, W.; Cha, H.
Data sourcing, collection, paper writing-original and review: Choi, S.
Supervision, paper writing-original and review: Song, G.

### Availability of data and materials

Not applicable.

### Financial support and sponsorship

This work was supported by National Research Council of Science & Technology (NST) grant by the Korea Government (MSIT) (No. GTL24011-000) and the Technology Innovation Program (2410009665, Development of integrated battery cell manufacturing process and reliability evaluation technology using high-speed/low-energy curing technology) through the Korea Planning & Evaluation Institute of Industrial Technology (KEIT) funded by the Ministry of Trade, Industry & Energy (MOTIE, Korea).

### Conflicts of interest

All authors declared that there are no conflicts of interest.

### Ethical approval and consent to participate

Not applicable.

### Consent for publication

Not applicable.



## REFERENCES

1. Grey, C. P.; Hall, D. S. Prospects for lithium-ion batteries and beyond-a 2030 vision. *Nat. Commun.* **2020**, *11*, 6279. DOI PubMed PMC
2. Kim, T.; Song, W.; Son, D. Y.; Ono, L. K.; Qi, Y. Lithium-ion batteries: outlook on present, future, and hybridized technologies. *J. Mater. Chem. A.* **2019**, *7*, 2942-64. DOI
3. Frith, J. T.; Lacey, M. J.; Ulissi, U. A non-academic perspective on the future of lithium-based batteries. *Nat. Commun.* **2023**, *14*, 420. DOI PubMed PMC
4. Manthiram, A. A reflection on lithium-ion battery cathode chemistry. *Nat. Commun.* **2020**, *11*, 1550. DOI PubMed PMC
5. Murdock, B. E.; Toghill, K. E.; Tapia-Ruiz, N. A perspective on the sustainability of cathode materials used in lithium-ion batteries. *Adv. Energy. Mater.* **2021**, *11*, 2102028. DOI
6. Stallard, J. C.; Wheatcroft, L.; Booth, S. G.; et al. Mechanical properties of cathode materials for lithium-ion batteries. *Joule* **2022**, *6*, 984-1007. DOI
7. Li, W.; Erickson, E. M.; Manthiram, A. High-nickel layered oxide cathodes for lithium-based automotive batteries. *Nat. Energy.*

**2020**, *5*, 26-34. DOI

8. Wu, F.; Yushin, G. Conversion cathodes for rechargeable lithium and lithium-ion batteries. *Energy. Environ. Sci.* **2017**, *10*, 435-59. DOI
9. Yu, S. H.; Feng, X.; Zhang, N.; Seok, J.; Abruña, H. D. Understanding conversion-type electrodes for lithium rechargeable batteries. *ACC. Chem. Res.* **2018**, *51*, 273-81. DOI
10. Schipper, F.; Erickson, E. M.; Erk, C.; Shin, J. Y.; Chesneau, F. F.; Aurbach, D. Review - recent advances and remaining challenges for lithium ion battery cathodes: I. Nickel-rich, $LiNi_xCo_yMn_zO_2$. *J. Electrochem. Soc.* **2017**, *164*, A6220-8. DOI
11. European Commission. Light-duty vehicles. Available from: https://climate.ec.europa.eu/eu-action/transport-decarbonisation/road-transport/light-duty-vehicles_en [Last accessed on 26 Jun 2025].
12. Major policy issued in lithium battery industry to accelerate the elimination of low-end redundant capacity. 2024. Available from: https://www.energytrend.com/news/20240511-46916.html [Last accessed on 4 Jun 2025].
13. EV100 Forum: China's vision for new energy vehicle industry. 2024. Available from: https://carnewschina.com/2024/03/18/ev100-forum-chinas-vision-for-new-energy-vehicle-industry/ [Last accessed on 4 Jun 2025].
14. Buffie, N. E. The section 45X advanced manufacturing production credit. 2024. Available from: https://www.congress.gov/crs-product/IF12809 [Last accessed on 4 Jun 2025].
15. Yang, H. LG Chem to invest over $3 billion to build U.S. battery cathode plant. 2022. Available from: https://www.reuters.com/business/lg-chem-invest-more-than-3-bln-build-battery-cathode-plant-us-2022-11-21/ [Last accessed on 4 Jun 2025].
16. Ryu, M.; Hong, Y. K.; Lee, S. Y.; Park, J. H. Ultrahigh loading dry-process for solvent-free lithium-ion battery electrode fabrication. *Nat. Commun.* **2023**, *14*, 1316. DOI PubMed PMC
17. Jin, W.; Song, G.; Yoo, J. K.; Jung, S.; Kim, T. H.; Kim, J. Advancements in dry electrode technologies: towards sustainable and efficient battery manufacturing. *ChemElectroChem* **2024**, *11*, e202400288. DOI
18. Oh, H.; Kim, G. S.; Bang, J.; Kim, S.; Jeong, K. M. Dry-processed thick electrode design with a porous conductive agent enabling 20 mA h $cm^{-2}$ for high-energy-density lithium-ion batteries. *Energy. Environ. Sci.* **2025**, *18*, 645-58. DOI
19. Xue, W.; Huang, M.; Li, Y.; et al. Ultra-high-voltage Ni-rich layered cathodes in practical Li metal batteries enabled by a sulfonamide-based electrolyte. *Nat. Energy.* **2021**, *6*, 495-505. DOI
20. Yu, Z.; Tong, Q.; Cheng, Y.; et al. Enabling 4.6 V $LiNi_{0.6}Co_{0.2}Mn_{0.2}O_2$ cathodes with excellent structural stability: combining surface $LiLaO_2$ self-assembly and subsurface La-pillar engineering. *Energy. Mater.* **2022**, *2*, 200037. DOI
21. Cai, D.; Gao, M.; Luo, S.; et al. Scalable thick Ni-rich layered oxide cathode design for high energy/power balanced lithium-ion battery. *J. Power. Sources.* **2024**, *602*, 234276. DOI
22. Islam, M. S.; Fisher, C. A. Lithium and sodium battery cathode materials: computational insights into voltage, diffusion and nanostructural properties. *Chem. Soc. Rev.* **2014**, *43*, 185-204. DOI PubMed
23. Sallas, D. V. D. C.; Kawata, B. A.; Galão, O. F.; et al. The influence of synthesis temperature on the HT-$LiCoO_2$ crystallographic properties. *Semin. Ciênc. Exatas. Tecnol.* **2019**, *40*, 115. DOI
24. Entwistle, T.; Sanchez-Perez, E.; Murray, G. J.; Anthonisamy, N.; Cussen, S. A. Co-precipitation synthesis of nickel-rich cathodes for Li-ion batteries. *Energy. Rep.* **2022**, *8*, 67-73. DOI
25. Yang, J.; Guan, N.; Xu, C.; et al. The synthesis and modification of $LiFePO_4$ lithium-ion battery cathodes: a mini review. *CrystEngComm* **2024**, *26*, 3441-54. DOI
26. Meng, Z.; Ma, X.; Azhari, L.; Hou, J.; Wang, Y. Morphology controlled performance of ternary layered oxide cathodes. *Commun. Mater.* **2023**, *4*, 418. DOI
27. Erabhoina, H.; Thelakkat, M. Tuning of composition and morphology of $LiFePO_4$ cathode for applications in all solid-state lithium metal batteries. *Sci. Rep.* **2022**, *12*, 5454. DOI PubMed PMC
28. Wang, Y.; Shadow Huang, H. Y. An overview of lithium-ion battery cathode materials. *MRS. Online. Proc. library.* **2011**, *1363*, 530. DOI
29. Saldaña, G.; San Martín, J. I.; Zamora, I.; Asensio, F. J.; Oñederra, O. Analysis of the current electric battery models for electric vehicle simulation. *Energies* **2019**, *12*, 2750. DOI
30. Kim, N.; Shamim, N.; Crawford, A.; et al. Comparison of Li-ion battery chemistries under grid duty cycles. *J. Power. Sources.* **2022**, *546*, 231949. DOI
31. Sadeghi, H.; Restuccia, F. Pyrolysis-based modelling of 18650-type lithium-ion battery fires in thermal runaway with LCO, LFP and NMC cathodes. *J. Power. Sources.* **2024**, *603*, 234480. DOI
32. Fallah, N.; Fitzpatrick, C. Is shifting from Li-ion NMC to LFP in EVs beneficial for second-life storages in electricity markets? *J. Energy. Storage.* **2023**, *68*, 107740. DOI
33. Tim, H.; Christoph, N.; Inés, R. I.; et al. Lithium-ion battery roadmap - industrialization perspectives toward 2030. DOI
34. Sun, Y. K. High-capacity layered cathodes for next-generation electric vehicles. *ACS. Energy. Lett.* **2019**, *4*, 1042-4. DOI
35. Jin, W.; Kim, Y.; Jang, H.; et al. Identifying the nanostructure of residual Li in high-Ni cathodes for lithium-ion batteries. *J. Mater. Chem. A.* **2025**, *13*, 5599-605. DOI
36. Tian, Q.; Song, R.; Zhang, J.; et al. Formation mechanism and removal strategy of residual lithium compounds on nickel-rich cathode materials. *Prog. Nat. Sci. Mater. Int.* **2024**, *34*, 1158-66. DOI
37. Sim, Y. B.; Lee, H.; Mun, J.; Kim, K. J. Modification strategies improving the electrochemical and structural stability of high-Ni cathode materials. *J. Energy. Chem.* **2024**, *96*, 185-205. DOI

38. Liu, T.; Yu, L.; Lu, J.; et al. Rational design of mechanically robust Ni-rich cathode materials via concentration gradient strategy. *Nat. Commun.* **2021**, *12*, 6024. DOI PubMed PMC
39. Yoon, C. S.; Park, K.; Kim, U.; Kang, K. H.; Ryu, H.; Sun, Y. High-energy Ni-rich $Li[Ni_xCo_yMn_{1-x-y}]O_2$ cathodes via compositional partitioning for next-generation electric vehicles. *Chem. Mater.* **2017**, *29*, 10436-45. DOI
40. Liu, W.; Oh, P.; Liu, X.; et al. Nickel-rich layered lithium transition-metal oxide for high-energy lithium-ion batteries. *Angew. Chem. Int. Ed.* **2015**, *54*, 4440-57. DOI
41. Manthiram, A.; Song, B.; Li, W. A perspective on nickel-rich layered oxide cathodes for lithium-ion batteries. *Energy. Storage. Mater.* **2017**, *6*, 125-39. DOI
42. Ko, D. S.; Park, J. H.; Yu, B. Y.; et al. Degradation of high-nickel-layered oxide cathodes from surface to bulk: a comprehensive structural, chemical, and electrical analysis. *Adv. Energy. Mater.* **2020**, *10*, 2001035. DOI
43. Kim, J.; Lee, H.; Cha, H.; Yoon, M.; Park, M.; Cho, J. Prospect and reality of Ni-rich cathode for commercialization. *Adv. Energy. Mater.* **2018**, *8*, 1702028. DOI
44. Kim, J. H.; Ryu, H. H.; Kim, S. J.; Yoon, C. S.; Sun, Y. K. Degradation mechanism of highly Ni-rich $Li[Ni_xCo_yMn_{1-x-y}]O_2$ cathodes with $x > 0.9$. *ACS. Appl. Mater. Interfaces.* **2019**, *11*, 30936-42. DOI
45. Xu, C.; Märker, K.; Lee, J.; et al. Bulk fatigue induced by surface reconstruction in layered Ni-rich cathodes for Li-ion batteries. *Nat. Mater.* **2021**, *20*, 84-92. DOI
46. Wu, F.; Tian, J.; Su, Y.; et al. Effect of $Ni^{2+}$ content on lithium/nickel disorder for Ni-rich cathode materials. *ACS. Appl. Mater. Interfaces.* **2015**, *7*, 7702-8. DOI
47. He, T.; Chen, L.; Su, Y.; et al. The effects of alkali metal ions with different ionic radii substituting in Li sites on the electrochemical properties of Ni-Rich cathode materials. *J. Power. Sources.* **2019**, *441*, 227195. DOI
48. Lin, Q.; Guan, W.; Meng, J.; et al. A new insight into continuous performance decay mechanism of Ni-rich layered oxide cathode for high energy lithium ion batteries. *Nano. Energy.* **2018**, *54*, 313-21. DOI
49. Shi, T.; Liu, F.; Liu, W.; et al. Cation mixing regulation of cobalt-free high-nickel layered cathodes enables stable and high-rate lithium-ion batteries. *Nano. Energy.* **2024**, *123*, 109410. DOI
50. Wu, F.; Liu, N.; Chen, L.; et al. Improving the reversibility of the H2-H3 phase transitions for layered Ni-rich oxide cathode towards retarded structural transition and enhanced cycle stability. *Nano. Energy.* **2019**, *59*, 50-7. DOI
51. Ryu, H. H.; Park, K. J.; Yoon, C. S.; Sun, Y. K. Capacity fading of Ni-rich $Li[Ni_xCo_yMn_{1-x-y}]O_2$ ($0.6 \leq x \leq 0.95$) cathodes for high-energy-density lithium-ion batteries: bulk or surface degradation? *Chem. Mater.* **2018**, *30*, 1155-63. DOI
52. Cho, D. H.; Jo, C. H.; Cho, W.; et al. Effect of residual lithium compounds on layer Ni-rich $Li[Ni_{0.7}Mn_{0.3}]O_2$. *J. Electrochem. Soc.* **2014**, *161*, A920-6. DOI
53. Jo, C. H.; Cho, D. H.; Noh, H. J.; Yashiro, H.; Sun, Y. K.; Myung, S. T. An effective method to reduce residual lithium compounds on Ni-rich $Li[Ni_{0.6}Co_{0.2}Mn_{0.2}]O_2$ active material using a phosphoric acid derived $Li_3PO_4$ nanolayer. *Nano. Res.* **2015**, *8*, 1464-79. DOI
54. Ross, G.; Watts, J.; Hill, M.; Morrissey, P. Surface modification of poly(vinylidene fluoride) by alkaline treatment1. The degradation mechanism. *Polymer* **2000**, *41*, 1685-96. DOI
55. Xiang, J.; Wei, Y.; Zhong, Y.; et al. Building practical high-voltage cathode materials for lithium-ion batteries. *Adv. Mater.* **2022**, *34*, e2200912. DOI
56. Zhang, Y.; Katayama, Y.; Tatara, R.; et al. Revealing electrolyte oxidation *via* carbonate dehydrogenation on Ni-based oxides in Li-ion batteries by *in situ* Fourier transform infrared spectroscopy. *Energy. Environ. Sci.* **2020**, *13*, 183-99. DOI
57. Giordano, L.; Karayaylali, P.; Yu, Y.; et al. Chemical reactivity descriptor for the oxide-electrolyte interface in Li-ion batteries. *J. Phys. Chem. Lett.* **2017**, *8*, 3881-7. DOI
58. Yu, Y.; Karayaylali, P.; Katayama, Y.; et al. Coupled $LiPF_6$ decomposition and carbonate dehydrogenation enhanced by highly covalent metal oxides in high-energy Li-ion batteries. *J. Phys. Chem. C.* **2018**, *122*, 27368-82. DOI
59. Wu, F.; Dong, J.; Chen, L.; et al. High-voltage and high-safety nickel-rich layered cathode enabled by a self-reconstructive cathode/electrolyte interphase layer. *Energy. Storage. Mater.* **2021**, *41*, 495-504. DOI
60. Sharifi-Asl, S.; Lu, J.; Amine, K.; Shahbazian-Yassar, R. Oxygen release degradation in Li-ion battery cathode materials: mechanisms and mitigating approaches. *Adv. Energy. Mater.* **2019**, *9*, 1900551. DOI
61. Li, Y.; Liu, X.; Wang, L.; et al. Thermal runaway mechanism of lithium-ion battery with $LiNi_{0.8}Mn_{0.1}Co_{0.1}O_2$ cathode materials. *Nano. Energy.* **2021**, *85*, 105878. DOI
62. Gallus, D. R.; Schmitz, R.; Wagner, R.; et al. The influence of different conducting salts on the metal dissolution and capacity fading of NCM cathode material. *Electrochim. Acta.* **2014**, *134*, 393-8. DOI
63. Liu, X.; Ren, D.; Hsu, H.; et al. Thermal runaway of lithium-ion batteries without internal short circuit. *Joule* **2018**, *2*, 2047-64. DOI
64. Yang, X. G.; Liu, T.; Wang, C. Y. Thermally modulated lithium iron phosphate batteries for mass-market electric vehicles. *Nat. Energy.* **2021**, *6*, 176-85. DOI
65. Xia, Y.; Zheng, J.; Wang, C.; Gu, M. Designing principle for Ni-rich cathode materials with high energy density for practical applications. *Nano. Energy.* **2018**, *49*, 434-52. DOI
66. Kim, Y.; Kim, M.; Lee, T.; et al. Investigation of mass loading of cathode materials for high energy lithium-ion batteries. *Electrochem. Commun.* **2023**, *147*, 107437. DOI
67. Kuang, Y.; Chen, C.; Kirsch, D.; Hu, L. Thick electrode batteries: principles, opportunities, and challenges. *Adv. Energy. Mater.*

**2019**, *9*, 1901457. DOI

68. Zhou, C. C.; Su, Z.; Gao, X. L.; Cao, R.; Yang, S. C.; Liu, X. H. Ultra-high-energy lithium-ion batteries enabled by aligned structured thick electrode design. *Rare. Met.* **2022**, *41*, 14-20. DOI
69. Lombardo, T.; Ngandjong, A. C.; Belhcen, A.; Franco, A. A. Carbon-binder migration: a three-dimensional drying model for lithium-ion battery electrodes. *Energy. Storage. Mater.* **2021**, *43*, 337-47. DOI
70. Ogihara, N.; Itou, Y.; Sasaki, T.; Takeuchi, Y. Impedance spectroscopy characterization of porous electrodes under different electrode thickness using a symmetric cell for high-performance lithium-ion batteries. *J. Phys. Chem. C.* **2015**, *119*, 4612-9. DOI
71. Park, K. Y.; Park, J. W.; Seong, W. M.; et al. Understanding capacity fading mechanism of thick electrodes for lithium-ion rechargeable batteries. *J. Power. Sources.* **2020**, *468*, 228369. DOI
72. Li, S.; Tian, G.; Xiong, R.; et al. Enhanced homogeneity of electrochemical reaction via low tortuosity enabling high-voltage nickel-rich layered oxide thick-electrode. *Energy. Storage. Mater.* **2022**, *46*, 443-51. DOI
73. Yan, Z.; Wang, L.; Zhang, H.; He, X. Determination and engineering of Li-ion tortuosity in electrode toward high performance of Li-ion batteries. *Adv. Energy. Mater.* **2024**, *14*, 2303206. DOI
74. Abdollahifar, M.; Cavers, H.; Scheffler, S.; Diener, A.; Lippke, M.; Kwade, A. Insights into influencing electrode calendering on the battery performance. *Adv. Energy. Mater.* **2023**, *13*, 2300973. DOI
75. Lu, X.; Daemi, S. R.; Bertei, A.; et al. Microstructural evolution of battery electrodes during calendering. *Joule* **2020**, *4*, 2746-68. DOI
76. Günther, T.; Schreiner, D.; Metkar, A.; Meyer, C.; Kwade, A.; Reinhart, G. Classification of calendering-induced electrode defects and their influence on subsequent processes of lithium-ion battery production. *Energy. Technol.* **2020**, *8*, 1900026. DOI
77. Cha, H.; Kim, J.; Lee, H.; et al. Boosting reaction homogeneity in high-energy lithium-ion battery cathode materials. *Adv. Mater.* **2020**, *32*, e2003040. DOI
78. Zhang, J.; Sun, J.; Huang, H.; Ji, C.; Yan, M.; Yuan, Z. Deformation and fracture mechanisms in the calendering process of lithium-ion battery electrodes. *Appl. Energy.* **2024**, *373*, 123900. DOI
79. Klein, S.; Bärmann, P.; Beuse, T.; et al. Exploiting the degradation mechanism of NCM523 graphite lithium-ion full cells operated at high voltage. *ChemSusChem* **2021**, *14*, 595-613. DOI
80. Song, Y.; Wang, L.; Sheng, L.; et al. The significance of mitigating crosstalk in lithium-ion batteries: a review. *Energy. Environ. Sci.* **2023**, *16*, 1943-63. DOI
81. Tsunekawa, H.; Tanimoto, A. S.; Marubayashi, R.; Fujita, M.; Kifune, K.; Sano, M. Capacity fading of graphite electrodes due to the deposition of manganese ions on them in Li-ion batteries. *J. Electrochem. Soc.* **2002**, *149*, A1326. DOI
82. Zheng, H.; Sun, Q.; Liu, G.; Song, X.; Battaglia, V. S. Correlation between dissolution behavior and electrochemical cycling performance for $LiNi_{1/3}Co_{1/3}Mn_{1/3}O_2$-based cells. *J. Power. Sources.* **2012**, *207*, 134-40. DOI
83. Komaba, S.; Kumagai, N.; Kataoka, Y. Influence of manganese(II), cobalt(II), and nickel(II) additives in electrolyte on performance of graphite anode for lithium-ion batteries. *Electrochim. Acta.* **2002**, *47*, 1229-39. DOI
84. Kim, J.; Ma, H.; Cha, H.; et al. A highly stabilized nickel-rich cathode material by nanoscale epitaxy control for high-energy lithium-ion batteries. *Energy. Environ. Sci.* **2018**, *11*, 1449-59. DOI
85. Zhang, X.; Cui, Z.; Manthiram, A. Insights into the crossover effects in cells with high-nickel layered oxide cathodes and silicon/graphite composite anodes. *Adv. Energy. Mater.* **2022**, *12*, 2103611. DOI
86. Moon, J.; Lee, H. C.; Jung, H.; et al. Interplay between electrochemical reactions and mechanical responses in silicon-graphite anodes and its impact on degradation. *Nat. Commun.* **2021**, *12*, 2714. DOI PubMed PMC
87. Kim, M.; Yang, Z.; Trask, S. E.; Bloom, I. Understanding the effect of cathode composition on the interface and crosstalk in NMC/Si full cells. *ACS. Appl. Mater. Interfaces.* **2022**, *14*, 15103-11. DOI
88. Zhang, X.; Wang, A.; Liu, X.; Luo, J. Dendrites in lithium metal anodes: suppression, regulation, and elimination. *Acc. Chem. Res.* **2019**, *52*, 3223-32. DOI
89. Yamaki, J.; Tobishima, S.; Hayashi, K.; Keiichi, S.; Nemoto, Y.; Arakawa, M. A consideration of the morphology of electrochemically deposited lithium in an organic electrolyte. *J. Power. Sources.* **1998**, *74*, 219-27. DOI
90. Langdon, J.; Manthiram, A. Crossover effects in batteries with high-nickel cathodes and lithium-metal anodes. *Adv. Funct. Mater.* **2021**, *31*, 2010267. DOI
91. Langdon, J.; Manthiram, A. Crossover effects in lithium-metal batteries with a localized high concentration electrolyte and high-nickel cathodes. *Adv. Mater.* **2022**, *34*, e2205188. DOI PubMed
92. Li, F.; Liu, Z.; Liao, C.; Xu, X.; Zhu, M.; Liu, J. Gradient boracic polyanion doping-derived surface lattice modulation of high-voltage Ni-rich layered cathodes for high-energy-density Li-ion batteries. *ACS. Energy. Lett.* **2023**, *8*, 4903-14. DOI
93. Xu, C.; Reeves, P. J.; Jacquet, Q.; Grey, C. P. Phase behavior during electrochemical cycling of Ni-rich cathode materials for Li-ion batteries. *Adv. Energy. Mater.* **2021**, *11*, 2003404. DOI
94. Jiang, Z.; Yang, T.; Li, C.; et al. Synergistic additives enabling stable cycling of ether electrolyte in 4.4 V Ni-rich/Li metal batteries. *Adv. Funct. Mater.* **2023**, *33*, 2306868. DOI
95. Zhang, J.; Zhang, H.; Deng, L.; et al. An additive-enabled ether-based electrolyte to realize stable cycling of high-voltage anode-free lithium metal batteries. *Energy. Storage. Mater.* **2023**, *54*, 450-60. DOI
96. Ren, X.; Zou, L.; Jiao, S.; et al. High-concentration ether electrolytes for stable high-voltage lithium metal batteries. *ACS. Energy. Lett.* **2019**, *4*, 896-902. DOI

97. Li, Z.; Rao, H.; Atwi, R.; et al. Non-polar ether-based electrolyte solutions for stable high-voltage non-aqueous lithium metal batteries. *Nat. Commun.* **2023**, *14*, 868. DOI PubMed PMC
98. Mao, M.; Gong, L.; Wang, X.; et al. Electrolyte design combining fluoro- with cyano-substitution solvents for anode-free Li metal batteries. *Proc. Natl. Acad. Sci. USA.* **2024**, *121*, e2316212121. DOI PubMed PMC
99. Günter, F. J.; Wassiliadis, N. State of the art of lithium-ion pouch cells in automotive applications: cell teardown and characterization. *J. Electrochem. Soc.* **2022**, *169*, 030515. DOI
100. Embleton, T. J.; Choi, J. H.; Won, S.; et al. High-energy density ultra-thick drying-free Ni-rich cathode electrodes for application in Lithium-ion batteries. *Energy. Storage. Mater.* **2024**, *71*, 103542. DOI
101. Kim, J. H.; Lee, K. M.; Kim, J. W.; et al. Regulating electrostatic phenomena by cationic polymer binder for scalable high-areal-capacity Li battery electrodes. *Nat. Commun.* **2023**, *14*, 5721. DOI PubMed PMC
102. Kim, J. H.; Kim, J. M.; Cho, S. K.; Kim, N. Y.; Lee, S. Y. Redox-homogeneous, gel electrolyte-embedded high-mass-loading cathodes for high-energy lithium metal batteries. *Nat. Commun.* **2022**, *13*, 2541. DOI PubMed PMC
103. Li, J.; Fleetwood, J.; Hawley, W. B.; Kays, W. From materials to cell: state-of-the-art and prospective technologies for lithium-ion battery electrode processing. *Chem. Rev.* **2022**, *122*, 903-56. DOI PubMed
104. Yao, W.; Chouchane, M.; Li, W.; et al. A 5 V-class cobalt-free battery cathode with high loading enabled by dry coating. *Energy. Environ. Sci.* **2023**, *16*, 1620-30. DOI
105. Kim, J.; Park, K.; Kim, M.; et al. 10 mAh $cm^{-2}$ cathode by roll-to-roll process for low cost and high energy density Li-ion batteries. *Adv. Energy. Mater.* **2024**, *14*, 2303455. DOI
106. Klein, S.; Harte, P.; van Wickeren, S.; et al. Re-evaluating common electrolyte additives for high-voltage lithium ion batteries. *Cell. Rep. Phys. Sci.* **2021**, *2*, 100521. DOI
107. Klein, S.; Wrogemann, J. M.; van Wickeren, S.; et al. Understanding the role of commercial separators and their reactivity toward $LiPF_6$ on the failure mechanism of high-voltage NCM523||graphite lithium ion cells. *Adv. Energy. Mater.* **2022**, *12*, 2102599. DOI
108. Klein, S.; van Wickeren, S.; Röser, S.; et al. Understanding the outstanding high-voltage performance of NCM523||graphite lithium ion cells after elimination of ethylene carbonate solvent from conventional electrolyte. *Adv. Energy. Mater.* **2021**, *11*, 2003738. DOI
109. Park, S.; Jeong, S. Y.; Lee, T. K.; et al. Replacing conventional battery electrolyte additives with dioxolone derivatives for high-energy-density lithium-ion batteries. *Nat. Commun.* **2021**, *12*, 838. DOI
110. Mao, M.; Ji, X.; Wang, Q.; et al. Anion-enrichment interface enables high-voltage anode-free lithium metal batteries. *Nat. Commun.* **2023**, *14*, 1082. DOI PubMed PMC
111. Li, N.; Gao, K.; Fan, K.; et al. Customization nanoscale interfacial solvation structure for low-temperature lithium metal batteries. *Energy. Environ. Sci.* **2024**, *17*, 5468-79. DOI
112. Lee, H.; An, H.; Chang, H.; et al. Boosting interfacial kinetics in extremely fast rechargeable Li-ion batteries with linear carbonate-based, $LiPF_6$-concentrated electrolyte. *Energy. Storage. Mater.* **2023**, *63*, 102995. DOI
113. Song, G.; Hwang, C.; Song, W. J.; et al. Breathable artificial interphase for dendrite-free and chemo-resistive lithium metal anode. *Small* **2022**, *18*, e2105724. DOI
114. Han, D. Y.; Song, G.; Kim, S.; Park, S. Dual-functional stacked polymer fibers for stable lithium metal batteries in carbonate-based electrolytes. *Small. Struct.* **2022**, *3*, 2200120. DOI